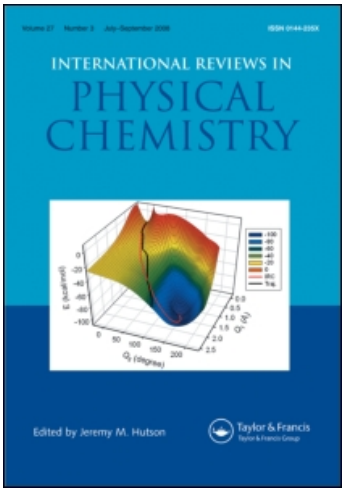

International Reviews in Physical Chemistry
Publication details, including instructions for authors and subscription information:
http://www.informaworld.com/smpp/title~content=t713724383

Infrared emission studies of the vibrational deactivation of benzene derivatives

John R. Barker[a]; Beatriz M. Toselli[b]
[a] Department of Atmospheric, Oceanic, and Space Sciences, Department of Chemistry, and Space Physics Research Laboratory, The University of Michigan, Ann Arbor, MN, USA [b] INFIQC, Departamento de Físicoquímica, Universidad Nacional de Córdoba, Córdoba, Argentina

To cite this Article Barker, John R. and Toselli, Beatriz M.(1993) 'Infrared emission studies of the vibrational deactivation of benzene derivatives', International Reviews in Physical Chemistry, 12: 2, 305 — 338
To link to this Article: DOI: 10.1080/01442359309353284
URL: http://dx.doi.org/10.1080/01442359309353284

INTERNATIONAL REVIEWS IN PHYSICAL CHEMISTRY, 1993, VOL. 12, NO. 2, 305–338

Infrared emission studies of the vibrational deactivation of benzene derivatives

by JOHN R. BARKER† and BEATRIZ M. TOSELLI‡

† Department of Atmospheric, Oceanic, and Space Sciences, Department of Chemistry, and Space Physics Research Laboratory, The University of Michigan, Ann Arbor, MN 48109-2143, USA

‡ INFIQC, Departamento de Físicoquímica, Universidad Nacional de Córdoba, Sucursal 16, C.C.61. 5016, Córdoba, Argentina

This paper reviews the time-resolved infrared fluorescence technique and its application to studies of the deactivation of highly vibrationally excited benzene-d_0, benzene-d_6, toluene-d_0, and toluene-d_8. The energy transfer parameters obtained are summarized in terms of both $\langle\langle \Delta E \rangle\rangle$ and $\langle \Delta E \rangle_d$, the average total energy transferred per collision and the average energy transferred in deactivating collisions, respectively. The mechanisms of energy transfer have also been investigated to determine the roles of vibration-to-translation/rotation and vibration-to-vibration energy transfer and the possible influence of quantum effects. The review concludes with a brief summary of a current view of large molecule energy transfer and suggestions for future work.

1. Introduction

In many non-equilibrium systems of fundamental and practical interest, collisional energy transfer involving highly excited polyatomic molecules plays an important role: in combustion, fuels are activated by collisions; in the atmosphere, recombination reactions require collisional stabilization; in laser-excited chemical systems, collisional energy transfer degrades and modifies the nascent population distributions. The theory of unimolecular and recombination reactions (herein grouped together as 'unimolecular reaction studies') is well developed (Robinson and Holbrook 1972, Forst 1973, Gilbert and Smith 1990), but it is deficient with respect to understanding large molecule collisional energy transfer (Quack and Troe 1977, Tardy and Rabinovitch 1977, Hippler and Troe 1989, Oref and Tardy 1990). Until energy transfer is understood on a more fundamental basis, quantitative theoretical prediction of pressure dependent unimolecular reaction rates will not be possible.

The understanding of energy transfer involving large, highly vibrationally excited polyatomic molecules is at a much earlier stage of development than that of small species at low energies (Lambert 1977, Yardley 1980, Krajnovich *et al.* 1987, Orr and Smith 1987). This is because large molecules have extremely large densities of states and a virtual continuum of eigenstates, while the small species at low excitation energies have states which are well-separated. While small species can be investigated on a state-to-state basis, large molecules must be investigated using less specific techniques. Nonetheless, small molecules provide a useful guide to understanding and anticipating large molecule behaviour.

In this review, we describe the infrared fluorescence (IRF) technique for investigating energy transfer in highly excited large molecules. The historical context surrounding the IRF technique is described in the next Section, followed by Sections outlining the theory involved, describing typical experimental arrangements, and summarizing

0144-235X/93 $10·00

important results obtained using the IRF technique to study benzene derivatives. In the final Section, we outline our current understanding of large molecule energy transfer and indicate some directions for future research.

2. A brief history of large molecule energy transfer

It is interesting to place the IRF technique in an historical context. This Section gives a subjective account of some of the principal influences on the IRF work carried out in this laboratory. More complete accounts of progress in energy transfer can be found elsewhere (Tardy and Rabinovitch 1977, Gilbert and Smith 1990).

Much early knowledge of energy transfer was derived from experimental unimolecular reaction studies, although some information was provided by physical techniques, such as ultrasonic dispersion (Cottrell and McCoubrey 1961). Prior to the development of chemical activation techniques, thermal unimolecular reaction systems provided most energy transfer information. Such thermal reaction systems are not ideal for energy transfer studies, because the distribution of excited species is controlled by the temperature and pressure, and the resulting distributions are relatively broad and are tied to the reaction threshold energy. The range of accessible temperatures is limited, because the chemical reaction must be competitive with collisional deactivation in order to obtain energy transfer information. The information derived from such experiments consists mostly of relative deactivation efficiencies of various colliders.

Chemical activation, which was extensively utilized by Rabinovitch and coworkers, was an improvement over thermal activation techniques. The chemically activated species is produced at a relatively high energy, so that reaction competes effectively with collisional deactivation at convenient pressures and at room temperature. Furthermore, the nascent chemical activation population distribution is much narrower than a thermal distribution with the same average energy. Using chemical activation, Rabinovitch and coworkers showed unambiguously that energy transfer takes place by 'weak collisions' and that the strong collision model of unimolecular reactions is merely a convenient limiting case (Tardy and Rabinovitch 1977, Gilbert and Smith 1990). They also developed practical numerical techniques for solving the master equation describing unimolecular reactions in collisional systems.

Photoactivation has also been used in unimolecular reaction studies. Atkinson and Thrush (1969, 1970) applied this technique to the investigation of the isomerization of 1,3,5-cycloheptatriene to produce toluene (also see Haller and Srinivasan (1965)). Their study was noteworthy because the highly vibrationally excited molecules in the electronic ground state were produced by fast radiationless transitions from the excited electronic state first populated by photon absorption. They modelled this system in the same way as chemical activation systems, but included only deactivating collisions; later a more refined model was employed (Rabinovitch *et al.* 1971). Subsequently, Troe and coworkers carried out extensive additional studies with cycloheptatriene derivatives (Luu and Troe 1974, Hippler and Troe 1989). The utilization of photoactivation and subsequent radiationless transitions is an essential part of most of the physical techniques now used for large molecule energy transfer studies.

Unimolecular reaction studies of energy transfer are hampered by several problems. The energy transfer manifests itself only in competition with the chemical reaction and thus the accuracy of the energy transfer parameters depends critically on knowledge of the energy dependent reaction rate constants. For example, if the reaction critical energy is set erroneously low, the unimolecular reaction rates will be

overestimated (assuming the Rice–Ramsperger–Kassel–Marcus (RRKM) theory is applicable) and the energy transfer will appear to be more effective than is actually the case. In unimolecular reaction studies it is also required that the chemical reaction mechanism be fully understood, but most reacting systems include numerous side-reactions and other complications which prevent full understanding. An additional limitation in unimolecular reaction systems is that energies below the reaction critical energy are inaccessible.

Because of the limitations of chemical reaction systems, various physical techniques have been developed to study energy transfer involving large molecules. For example, Neoporent investigated collisional energy transfer involving electronically excited β-naphthylamine by measuring the competition between spontaneous emission and collisional deactivation and modelling the system with a weak collision model similar to those used for unimolecular reactions (Neporent 1950, Neporent and Mirumyants 1960). An important feature of his work is that the energy dependence of the energy transfer was investigated by varying the photoexcitation wavelength. However, visible and ultraviolet fluorescence are not available for investigations of the electronic ground state, which is the subject of studies in our laboratory.

In our laboratory, we have utilized the time resolved IRF method for monitoring the deactivation of large molecules in their electronic ground states (Smith and Barker 1981, Rossi *et al.* 1983, Barker 1984)). This development was inspired by the use of IRF in investigations of small molecule energy transfer by George W. Flynn (Weitz and Flynn 1974) and C. Bradley Moore (1973), although the data analysis for large molecules differs greatly from that for small species. Another technique popularly used for this type of measurement is the time-resolved ultraviolet absorption (UVA) method, which was utilized for energy transfer measurements at almost the same time (Hippler *et al.* 1981, 1983, Nakashima and Yoshihara 1982, 1983). Both of these techniques use photoexcitation and rely on fast radiationless transitions from the excited electronic state to high vibrational levels of the ground electronic state. Both techniques are time resolved and require that the observed fluorescence or absorption be related to the vibrational energy resident in the excited molecule. In the UVA technique, calibrations are carried out by measuring the absorption spectra of shock-heated gases and obtaining an empirical relationship between the absorption coefficient and the average vibrational energy of the excited species. In the IRF technique, the infrared emission intensity is related to the microcanonical excitation energy of the excited species by a theoretical expression which has been tested in several experiments: no failures have yet been discovered, as discussed below.

Other physical techniques have also been developed recently to observe energy transfer involving large molecules: time-resolved tunable diode laser absorption (Jelenak *et al.* 1988, Chou *et al.* 1989, 1990, Sedlacek *et al.* 1991), and a method (Bevilacqua *et al.* 1990) for excited states based on the relative rates of radiationless transitions. All of these techniques provide information about the average energy transferred in collisions, but none of them provides much information about the shapes of the distribution functions. A newly-developed multiphoton ionization technique (Löhmannsröben and Luther 1988, Luther and Reihs 1988) is very promising in this regard. In the present paper, only the IRF technique is described in detail.

Prior to study of benzene and some of its derivatives, the IRF technique was applied to investigations of energy transfer involving azulene (Smith and Barker 1981, Rossi and Barker 1982, Rossi *et al.* 1983, Barker 1984, Barker and Golden 1984, Forst and Barker 1985, Shi and Barker 1988, Shi *et al.* 1988, Cherchneff and Barker 1989) and

1,1,2-trifluoroethane (Zellweger *et al.* 1985a, b, 1986). Azulene has very favorable photophysical properties, but it is not as easy to use as benzene. Most of the basic ideas behind the IRF technique were first tested using azulene, but the experimental data obtained using benzene derivatives is of much higher quality than the older azulene data. Partly, this is due to the greater ease of handling the benzene derivatives, compared to azulene, but mostly the improvement is due to the availability of better lasers and better signal acquisition equipment. The IRF data on energy transfer involving benzene derivatives is now one of the best available on energy transfer involving large molecules.

3. Theory

The master equation describing the evolution of population in a collisional system is the infinite set of coupled integro-differential equations:

$$\frac{\partial[N(E,t)]}{\partial t} = \int_0^\infty P_c(E,E')\omega[N(E',t)]\,\mathrm{d}E' - \omega[N(E,t)] + \sum_i^{\text{modes}} [N(E+h\nu_i,t)]A_i(E+h\nu_i) - \sum_i^{\text{modes}} [N(E,t)]A_i(E) - \sum_j^{\text{channels}} k_j(E)[N(E,t)]. \quad (1)$$

In his expression, $[N(E,t)]$ is the concentration of molecules with energy in the range E to $E+\mathrm{d}E$ at time t, $P_c(E,E')$ is the probability of a collisional transition from energy E' to energy E, ω is the collision frequency (which is assumed to be independent of excitation energy), and $A_i(E)$ is the energy-dependent rate coefficient for spontaneous emission by the ith emitting mode. The first term in equation (1) describes collisional production of $[N(E,t)]$ due to activation and deactivation of molecules initially at other energies. The second term describes the rate of loss of $[N(E,t)]$ due to collisions. The third term describes production of $[N(E,t)]$ by spontaneous emission by more highly excited molecules, and the fourth term similarly describes loss of population due to spontaneous emission. The fourth term is dominant in the limit of low pressures, leading to substantial stabilization, even when there are no collisions (Barker 1992). The last term accounts for unimolecular reaction of the excited molecules according to any number of reaction pathways, where the jth pathway has specific rate constant $k_j(E)$ which depends on excitation energy. Following Lindemann (1922), a term describing absorption of infrared radiation is usually neglected (except when considering infrared multiphoton pumping induced with a higher power laser), because the thermal radiation density at ordinary temperatures is very low.

In experimental systems (and in classical trajectory calculations) it is not possible to define precisely what is meant by a 'collision' and thus the individual factors in the first term of equation (1) cannot be separated, except for a linear density dependence. For convenience and for conceptual reasons, however, it is useful to separate them arbitrarily by defining the collision frequency and the step-size distribution. For a mixture of unexcited aromatic (termed the 'parent') and another gas (termed the 'collider'), the collision frequency experienced by an excited molecule is defined by

$$\omega = k_{LJ}^c[M] + k_{LJ}^p[P], \quad (2)$$

where k_{LJ}^i is the collision rate constant corresponding to collisions of the excited aromatic with collider ($i=c$), or parent ($i=p$), and $[M]$ and $[P]$ are the concentrations

of collider and parent gases, respectively. Conventionally, the rate constants are calculated for particles interacting according to the Lennard–Jones intermolecular potential (Kolmaier and Rabinovitch 1963); this convention is supported by classical trajectory calculations (Hippler and Troe 1989). All of the details of energy transfer are then contained in the step-size probability function $P_c(E, E')$, which is usually assumed to depend only on the bath gas temperature, the total energy of the excited molecule, and (sometimes) the energy of the collision partner. Numerous empirical models (Robinson and Holbrook 1972, Forst 1973, Tardy and Rabinovitch 1977, Barker 1983, Gilbert and Smith 1990) have been proposed for this function, including the stepladder, exponential, and reverse-exponential models, which are used with some regularity. Theoretical efforts have produced step-size distributions from ergodic collision theory, impulsive ergodic collision theory, and the biased random walk model, among others (Gilbert and Smith 1990, Gilbert 1991). Fortunately, numerical calculations have shown in many applications that the exact functional form of $P(E', E)$ is not very important. In the analysis of our experimental data, we have restricted ourselves to the exponential model, because there is no compelling theoretical or experimental reason to adopt anything more complex.

The rate coefficient for spontaneous emission by the ith vibrational mode, $A_i(E)$, depends on excitation energy, because the statistical probability of finding the appropriate amount of energy in the emitting mode is energy dependent. The fundamental expression for the power emitted per unit volume (J cm^{-3} s^{-1}) by the ith mode due to a transition from vibrational level v to level $v-1$ can be written

$$I_i(v) = h\nu_i A_i^{v,v-1}[N(i,v)], \tag{3}$$

where ν_i is the transition frequency, $A_i^{v,v-1}$ is the Einstein coefficient for spontaneous emission, and $[N(i,v)]$ is the concentration of molecules with v quanta in the ith mode.

Even for anharmonic molecules, most of the emission occurs by $\Delta v = -1$ transitions, which are accurately described by the harmonic oscillator approximation, where the Einstein coefficient for any $\Delta v = -1$ transition can be expressed in terms of the coefficient for the fundamental transition:

$$A_i^{v,v-1} = v_i A_i^{1,0}(\nu_{ai}/\nu_{hi})^3. \tag{4}$$

The last factor (Rawlins *et al.* 1985) is included to correct for anharmonicity, where ν_{ai} is the actual anharmonic frequency for the v to $v-1$ transition and ν_{hi} is the corresponding harmonic frequency, which may be taken as the observed $v=1$ to $v=0$ transition frequency. This anharmonic correction factor usually is nearly unity and can be neglected in most applications, especially if the density of states is calculated using harmonic oscillators (Brenner and Barker 1992b).

The concentration of molecules with v_i quanta in the ith mode can be written as the product of the total concentration of excited molecules $[N(E,t)]$ and $P_i(E,v)$, the probability of finding v quanta in the ith mode (the subscript is omitted from the quantum number to simplify notation). This probability is the ratio of the number of ways of distributing the energy in the molecule while constraining v quanta to reside in the ith mode, divided by the total number of ways of distribution of the energy. For a microcanonical system, the total number of ways of distributing the energy among s degrees of freedom is the product of the density of states at energy E multiplied by the differential of energy: $\rho_s(E)\,\mathrm{d}E$. Because there is only one way of putting v_i quanta in the ith mode and there are $\rho_{s-1}(E - v h\nu_i)$ ways of putting the remaining energy in the remaining modes, the total number of ways of distributing the energy with the

constraint is $\rho_{s-1}(E-vhv_i)\,dE$. Thus, the probability is given by (Durana and McDonald 1976)

$$P_i(E,v_i)=\frac{\rho_{s-1}(E-vhv_i)}{\rho_s(E)}, \tag{5}$$

and the rate coefficient for photon emission by the ith mode is

$$A_i(E)=\frac{I_i}{hv_i}\frac{1}{[N(E,t)]}=\frac{1}{\rho_s(E)}A_i^{1,0}\sum_{v_i=1}^{v_{max}}v_i\rho_{s-1}(E-v_ihv_i), \tag{6}$$

where the summation is over all vibrational levels allowed by conservation of energy.

Equation (6) not only describes the rate coefficient for infrared emission (Barker 1992), but it is also used for the analysis of infrared emission measurements of energy transfer. The emission observed in the experiments is proportional to the intensity emitted at all frequencies viewed by the detector (Durana and MacDonald 1976):

$$I(t)=\sum_i^{\text{modes}}I_i=\frac{[N(E,t)]}{\rho_s(E)}\sum_i^{\text{modes}}hv_iA_i^{1,0}\sum_{v_i=1}^{v_{max}}v_i\rho_{s-1}(E-v_ihv_i), \tag{7}$$

where the summation over i is restricted to the modes emitting within the range of the detector. In the IRF work in this laboratory, these modes are the C–H stretches ($\sim 3050\,cm^{-1}$) and the corresponding C–D stretches ($\sim 2250\,cm^{-1}$), which are well-separated in frequency from the other modes and are easily isolated with band-pass filters.

The validity of equation (7) has been verified by experiments involving several different emitting systems. Durana and MacDonald (1976) measured the relative IRF intensities for several infrared emitting modes in thermally excited molecules and the results agreed with equation (7) within a few per cent. In this laboratory, tests were carried out using azulene excited to high vibrational energies and the excellent agreement between equation (7) and the experiments is shown in figure 1 (Shi *et al.* 1988). Most recently, the emission spectrum of highly excited benzene was obtained (Brenner and Barker 1992a, b) and is presented in figure 2. The three components apparent in the emission spectrum are identified as $\Delta v=-1$ transition originating in upper vibrational levels $v=1$, 2, and 3. The relative intensities agree within $\sim 5\%$ with the individual vibrational terms in equation (7), which further supports its validity.

4. IRF experimental techniques

Details of experimental techniques can be found in several papers (Shi *et al.* 1988, Cherchneff and Barker 1989, Yerram *et al.* 1990, Toselli and Barker 1991, Toselli *et al.* 1991). An excimer laser (Lumonics HyperEx 440, uniform beam electrodes) irradiates the aromatic vapor in a 30 cm long, 4·5 cm diameter pyrex cell. Quartz windows are sealed to the cell with viton O-rings. IRF is viewed through a sapphire or quartz side window by a 3 mm diameter 77 K InSb photovoltaic detector (Infrared Associates) equipped with a matched preamplifier. The cell is pumped with a mercury-free gas handling system and the gas samples are introduced into the cell through a fine-control needle valve. Pressures are monitored with a 0–1 torr or 0–10 torr capacitance manometer (MKS Baratron model 227).

In some experiments, flowing conditions are achieved by cooling the reservoir with a cryogenic cooler (FTS Systems) to reduce the aromatic vapour pressures enough to achieve stable pressures in the flow cell, which is being pumped with a conventional

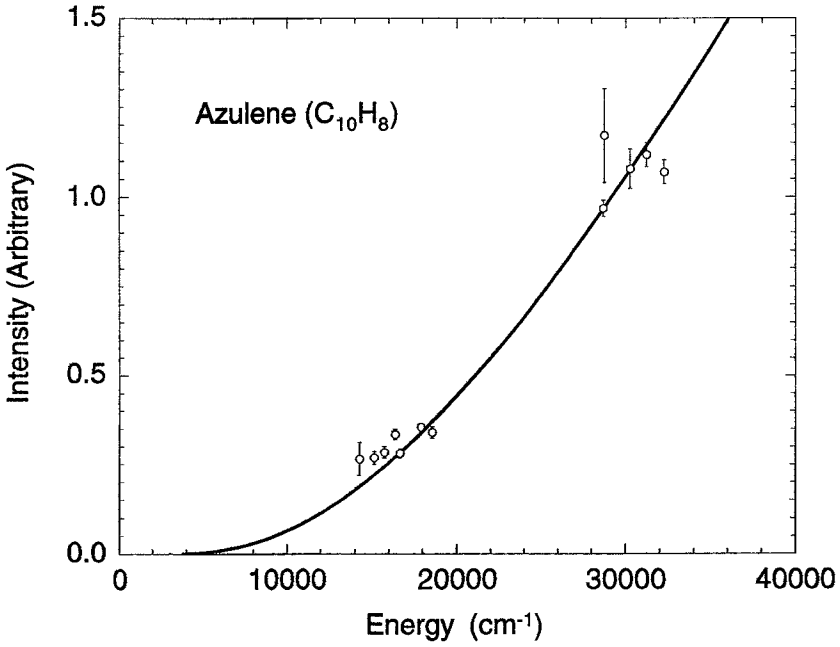

Figure 1. IRF calibration curve for azulene ($C_{10}H_8$) (Shi *et al.* 1988). Experimental points and uncertainties ($\pm 1\sigma$); solid line from equation (7), scaled to unity at 337 nm (29 674 cm^{-1}).

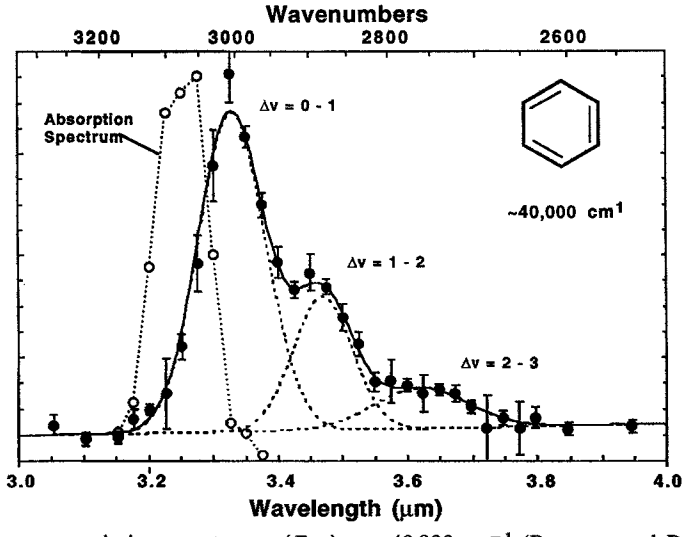

Figure 2. Benzene emission spectra at $\langle E_{vib} \rangle = \sim 40\,800\,cm^{-1}$ (Brenner and Barker 1992a). Experimental points (dark circles, $\pm 1\sigma$ error bars) and three-component Gaussian fits of the spectra are shown. Dotted lines show contributions of individual $\Delta v = -1$ transitions. Open circles joined by dots are vapour phase absorption data obtained with the same experimental apparatus as the emission spectrum.

vacuum line. In other experiments, static bulb conditions are used. Typically, mixtures contain ~5–10 mtorr of the aromatic and up to about 2 torr of collider.

The output of the infrared detector/preamplifier is further amplified (Tektronix AM502) and captured in some experiments with a transient recorder (Biomation 805) and summed by a signal averager (Nicolet 1070). In more recent experiments, the signals are captured and averaged by a digital oscilloscope (LeCroy 9400). The averaged signals are transferred to a laboratory computer (Digital Equipment Corp. LSI-11, or Apple Corp. Macintosh) for permanent storage on floppy disks and numerical analysis. The laser pulse repetition frequency is usually ~15 Hz for flowing conditions and ~40 Hz in the static bulb experiments. Signals are accumulated for 4000 to 16000 pulses, to achieve good signal-to-noise (S/N) ratios. The IRF signals are limited by the ~5 μs rise time of the infrared detector/preamplifier, and typical measured decay rates range from $<10^4\,s^{-1}$ to $\sim 10^5\,s^{-1}$. The IRF emission rates of isolated large molecules are typically $1–10^2\,s^{-1}$, and can be neglected at the pressures used in these experiments.

A slow decrease in aromatic partial pressures is sometimes observed while irradiating under static bulb conditions. A modulated molecular beam mass spectrometer (MMB-MS) detection technique (Zellweger *et al.* 1985a) is used to search for photoproducts in several different types of experiments. This technique discriminates against background and against species that scatter from the vacuum chamber walls subsequent to exiting the cell. Several modes of operation are possible with this experiment. For example, flow rates can be adjusted and the laser repetition frequency can be set low enough so that the cell empties between laser shots. At the other extreme, the cell can be closed and the gas irradiated by many laser pulses, and then analysed by the MMB-MS. Typically, only traces of H_2 have been detected as photoproducts (Yerram *et al.* 1990) and the MMB-MS enables quantitative measurements of the quantum yields of destruction in the experiments. For benzene derivatives, the quantum yields are a few per cent (Yerram *et al.* 1990, Tosseli and Barker 1991, Toselli *et al.* 1991) and do not constitute a significant source of problems, because energy remaining after photodissociation must be partitioned between the photofragments. Aromatic free radicals are likely to emit IRF near 3·3 μm and may contribute to the observed signal, but the radicals contain little energy and can make only small contributions, relative to the much more highly excited aromatic molecules (Toselli *et al.* 1991).

5. Experimental determination of energy transfer parameters

5.1. *Inversion of IRF data to obtain* $\langle\langle E\rangle\rangle_{inv}$ *and* $\langle\langle \Delta E\rangle\rangle_{inv}$

A typical set of fluorescence decay curves obtained for pure benzene at various pressures is shown in figure 3 (Yerram *et al.* 1990); the decay curves for other collider gases are similar, but have lower (S/N) ratios and the decays occur on different timescales. Due to the limited time response of the infrared detector, the intensity at $t=0$ is not observed directly, but must be obtained by back-extrapolation of a function fitted to the data obtained after the slow detector risetime (usually ~7 μs). These IRF decay curves, although approximately exponential, are well fitted by an empirical function using nonlinear least squares (Bevington 1969):

$$\langle\langle I(t)\rangle\rangle = A\exp(-k^I t + b^I t^2) + B, \tag{8}$$

where k^I and b^I are fitted parameters which depend on collider gas pressures. This expression was used to obtain a smooth empirical fit to the experimental data and to extrapolate the intensity to $t=0$.

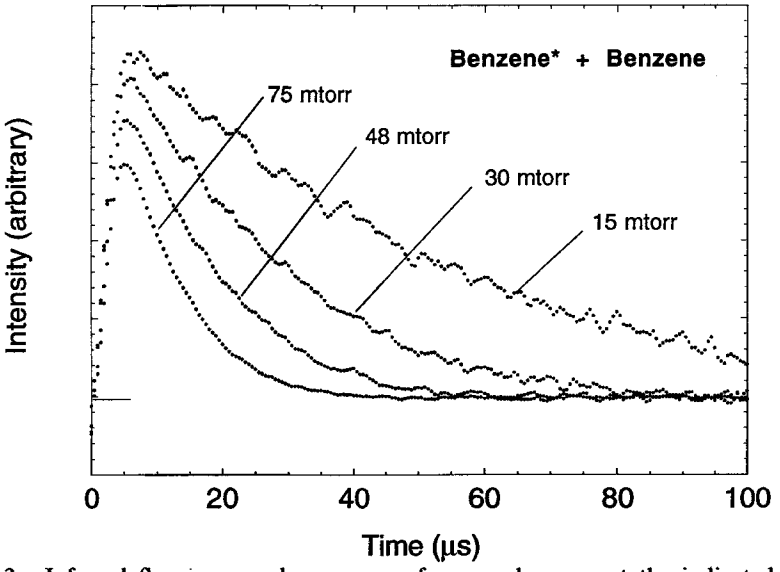

Figure 3. Infrared fluorescence decay curves for pure benzene at the indicated pressures (Yerram *et al.* 1990).

In order to relate the observed IRF signal to the vibrational energy content of the excited molecule, equation (7) was inverted and least-squares fitted to obtain the average vibrational energy as a function of the IRF intensity. Vibrational assignments for the aromatics were used with the Stein and Rabinovitch (1973) implementation of an algorithm (Beyer and Swinehaart 1973) for exact counts of states, as modified by Astholz *et al.* (1979) for free rotors. Examples of such least-squares fitted 'calibration curves' are given in table 1.

To convert the observed intensity decays to energy decays, knowledge of the initial energy is exploited to scale the experimental data so that the initial intensity corresponds to that calculated according to equation (7) at the initial energy (Toselli *et al.* 1991). The initial energy is taken to be the sum of the photon energy (40 320 cm^{-1}) and the average thermal vibrational energy of the aromatic at 300 K. The scaled experimental intensity data, or its least squares fit, can then be 'inverted' point-by-point to give the corresponding energy (Toselli *et al.* 1991).

The pressure-dependent data from figure 3 were inverted in this manner and replotted as a function of the total number of collisions ($Z=\omega t$) in figure 4: all of the experimental data 'collapse' onto the same line, which shows with good precision the average energy, $\langle\langle E\rangle\rangle$, as a function of the number of collisions, Z. To obtain the energy transfer parameters, these data are least-squares fitted and the derivative of $\langle\langle E\rangle\rangle$ with respect to the number of collisions gives $\langle\langle \Delta E\rangle\rangle$, the average energy transfer step size:

$$\frac{\mathrm{d}}{\mathrm{d}t}\langle\langle E\rangle\rangle=\omega\langle\langle \Delta E\rangle\rangle, \tag{9a}$$

$$\frac{\mathrm{d}}{\mathrm{d}Z}\langle\langle E\rangle\rangle=\langle\langle \Delta E\rangle\rangle. \tag{9b}$$

Here, the double brackets (Penner and Forst 1977) denote bulk averages of vibrational energy and energy transfer step sizes, k_{LJ} is the Lennard–Jones collision rate constant,

Table 1. IRF calibration functions: $\ln(E) = \sum_{k=0}^{4} a_k (\ln I')^k$.

Species	a_0	a_1	a_2	$10^3 a_3$	$10^5 a_4$
Benzene-d_0 (3073 cm^{-1})	11·6487	0·871	0·0767	2·93	—
Benzene-d_6 (2287 cm^{-1})	11·3351	0·871	0·0678	1·62	−2·55
Toluene-d_0 (3056 cm^{-1})	11·9241	0·897	0·0932	6·40	+22·6
Toluene-d_8 (2286 cm^{-1})	11·5804	0·853	0·0584	−1·07	−31·5

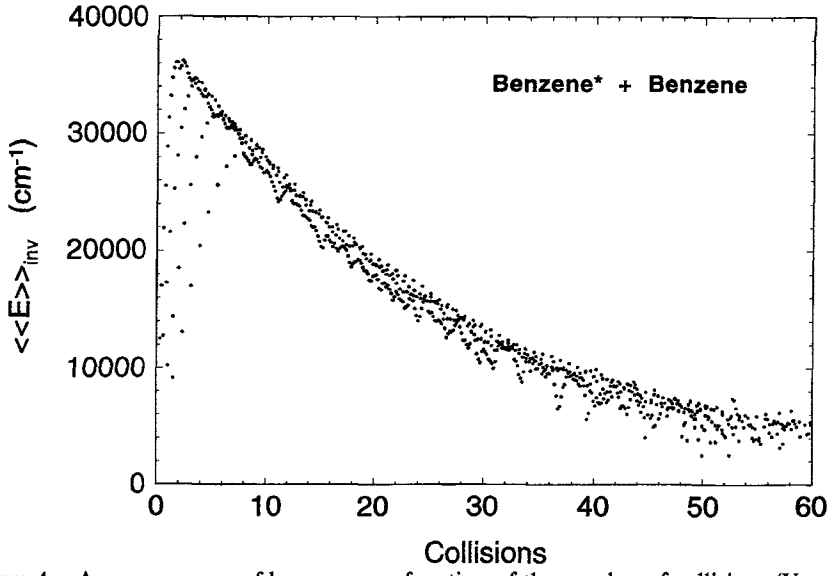

Figure 4. Average energy of benzene as a function of the number of collisions (Yerram *et al.* 1990).

$[M]$ is the number density of collider, and Z $(=\omega t)$ is the number of collisions. It is important to note that the product $\omega\langle\langle\Delta E\rangle\rangle$ appears in equation (9 *a*), and not the individual terms; the separation of this product into separate terms is arbitrary and is done for historical reasons and for convenience. In comparisons with other work, it may be necessary to adjust the values for $\langle\langle\Delta E\rangle\rangle$ to compensate for different choices of $k_{LJ}i$.

Note that the population distributions evolve with time and thus both $\langle\langle E\rangle\rangle$ and $\langle\langle\Delta E\rangle\rangle$ are time-dependent (Forst and Barker 1985, Yerram *et al.* 1990). Since both $\langle\langle E(t)\rangle\rangle$ and $\langle\langle\Delta E(t)\rangle\rangle$ are determined for the same instant of time from the experimental data, $\langle\langle\Delta E\rangle\rangle$ can be expressed as a function of $\langle\langle E\rangle\rangle$. To emphasize that the bulk average energies and step sizes were obtained from experimental data according to the inversion methods described in this Section, the subscript 'inv' is added: $\langle\langle E\rangle\rangle_{inv}$ and $\langle\langle\Delta E\rangle\rangle_{inv}$.

For experiments involving collider gases it is necessary to account for the effects of self-collisions (atomatic*–aromatic) in addition to collisions of excited aromatic with the collider gas. We have used various approaches to this problem, with varying degrees of success (Shi and Barker 1988, Yerram *et al.* 1990, Toselli *et al.* 1991). The procedure we currently feel to be the most effective is as follows (Toselli *et al.* 1991): (*a*)

every experimental decay curve is normalized individually so that its extrapolated intensity at $I(t=0)=I_0$ is equal to that calculated according to equation (7) at the initial energy; (*b*) the least squares fit of $\langle\langle I(t)\rangle\rangle$ against time is inverted through use of equations (7) and (8) to obtain $\langle\langle\Delta E\rangle\rangle_{inv}$ and $\langle\langle E\rangle\rangle_{inv}$ for the gas mixture; (*c*) for selected values of $\langle\langle E\rangle\rangle_{inv}$ (typically each $1000\,cm^{-1}$) curves are constructed of $\langle\langle\Delta E\rangle\rangle_{inv}$ against F_c, the fraction of collisions that occur with the collider gas:

$$F_c=\frac{[M]k_{LJ}^c}{k_{LJ}^c[M]+k_{LJ}^p[P]}=\frac{[M]k_{LJ}^c}{\omega}. \tag{10}$$

The next step is (*d*) to extrapolate to $\langle\langle\Delta E\rangle\rangle_{inv}$ at each energy to $F_c=1{\cdot}0$ to obtain $\langle\langle\Delta E\rangle\rangle_{inv}$ for the collider, uncontaminated by the effects of parent–parent gas collisions; (*e*) propagation of errors is carried out to estimate the uncertainties in $\langle\langle E\rangle\rangle_{inv}$ and $\langle\langle\Delta E\rangle_{inv}$. Note that instead of collision fraction, ordinary mole fraction could have been used for the extrapolation to pure collider, but plots of $\langle\langle\Delta E\rangle\rangle_{inv}$ against collision fraction are more nearly linear (mixtures that obey the 'linear mixing rule' produce strictly linear plots).

Figure 5 shows $\langle\langle\Delta E\rangle\rangle_{inv}$ as a function of F_c at selected average vibrational energies for the toluene*–SF_6 system (Toselli *et al.* 1991); extrapolation to $F_c=1$ gives $\langle\langle\Delta E\rangle\rangle_{inv}$ for toluene*–SF_6 collisions. The earliest portion of the experimental IRF decay curves is dominated by the limited time-response of the infrared detector and is omitted from further consideration (because of the relatively low *S/N* ratio in these experiments, it is not possible to numerically deconvolute the effect of the detector rise-time).

A selection of data evaluated according to this protocol for toluene-d_0 and toluene-d_8 is presented in figures 6–11. At low energies, the dependence of $\langle\langle\Delta E\rangle\rangle_{inv}$ on

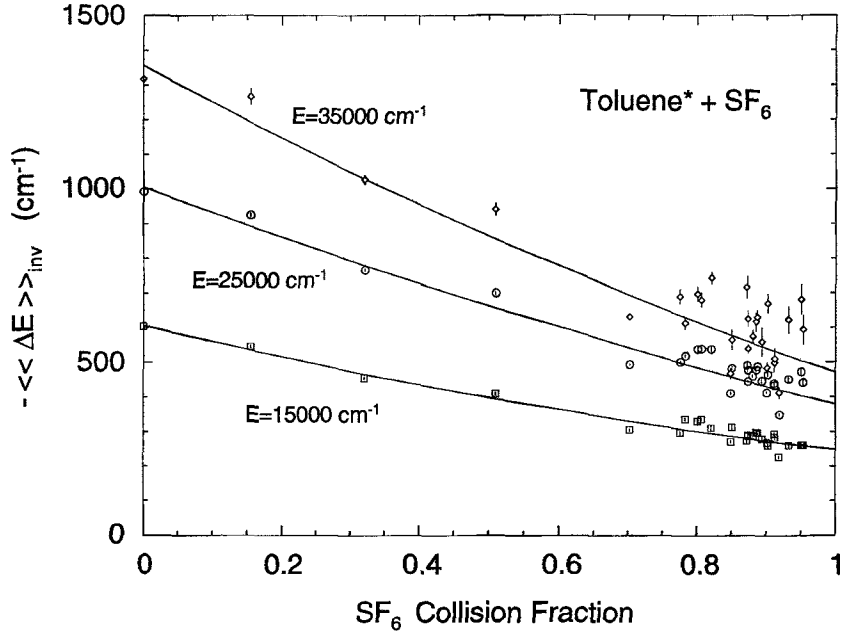

Figure 5. $-\langle\langle\Delta E\rangle\rangle_{inv}$ against collision fraction of SF_6 in deactivating excited toluene (for details, see Toselli *et al.* 1991).

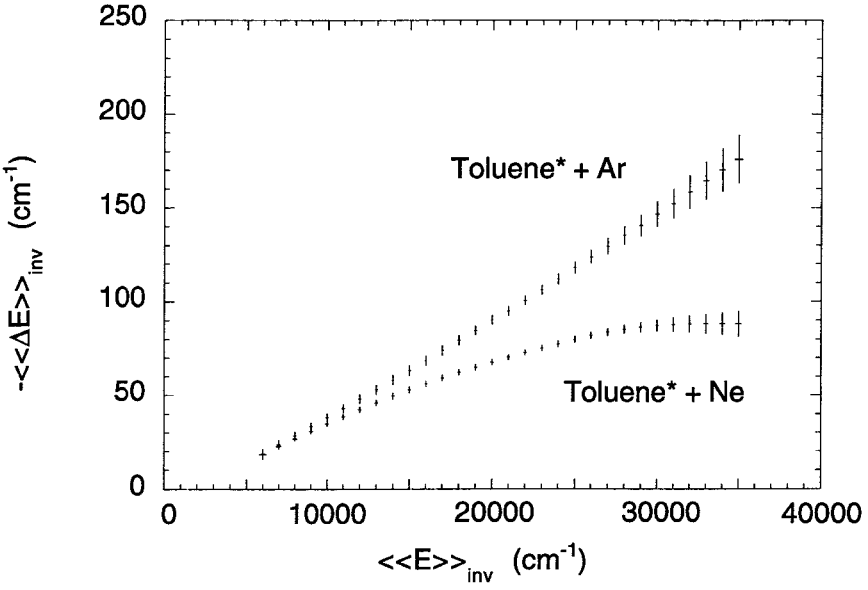

Figure 6. $-\langle\langle\Delta E\rangle\rangle_{inv}$ against $\langle\langle E\rangle\rangle_{inv}$ for deactivation of excited toluene-d_0 by some rare gases (Toselli *et al.* 1991). The error bars are $\pm 2\sigma$ statistical uncertainties.

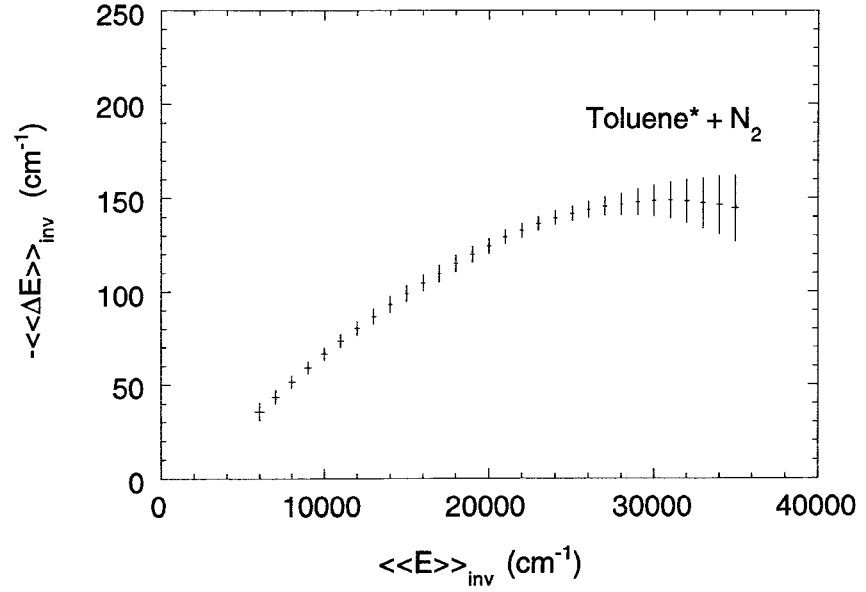

Figure 7. $-\langle\langle\Delta E\rangle\rangle_{inv}$ against $\langle\langle E\rangle\rangle_{inv}$ for deactivation of excited toluene-d_0 by nitrogen (Toselli *et al.* 1991).

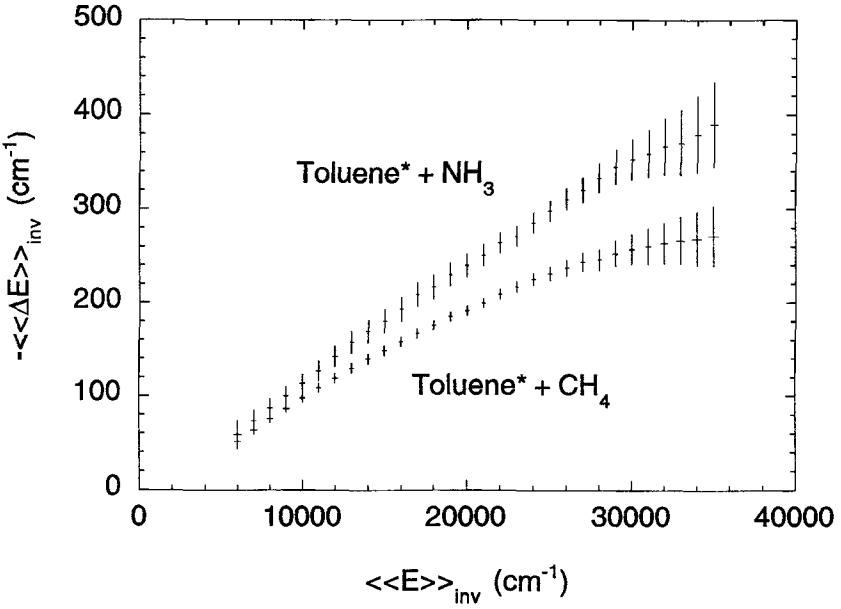

Figure 8. $-\langle\langle \Delta E \rangle\rangle_{inv}$ against $\langle\langle E \rangle\rangle_{inv}$ for deactivation of excited toluene-d_0 by ammonia and methane (Toselli *et al.* 1991).

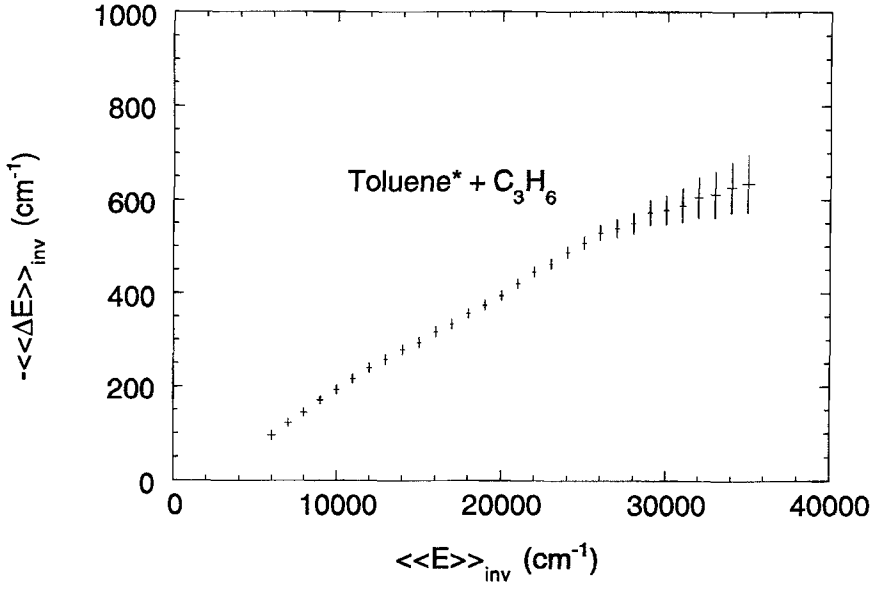

Figure 9. $-\langle\langle \Delta E \rangle\rangle_{inv}$ against $\langle\langle E \rangle\rangle_{inv}$ for deactivation of excited toluene-d_0 by propene (Toselli *et al.* 1991).

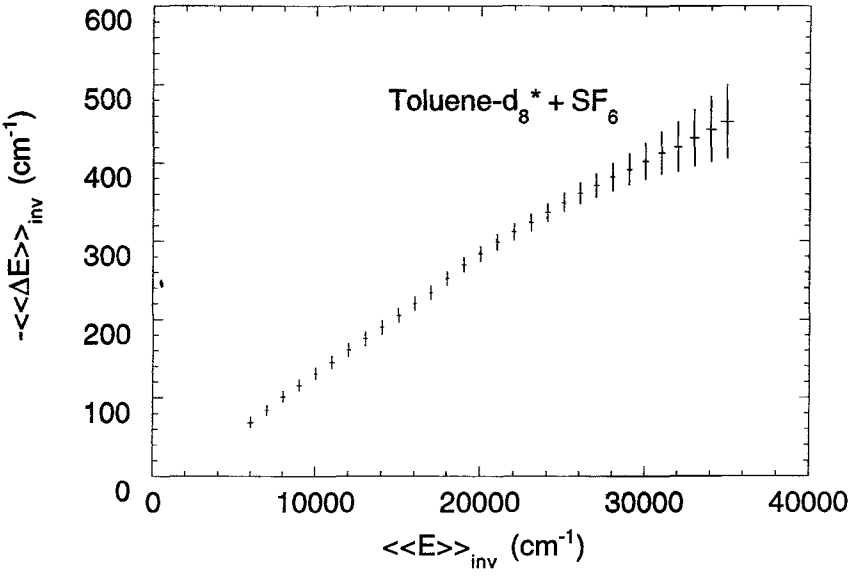

Figure 10. $-\langle\langle \Delta E \rangle\rangle_{inv}$ against $\langle\langle E \rangle\rangle_{inv}$ for deactivation of excited toluene-d_8 by SF_6 (Toselli and Barker 1992).

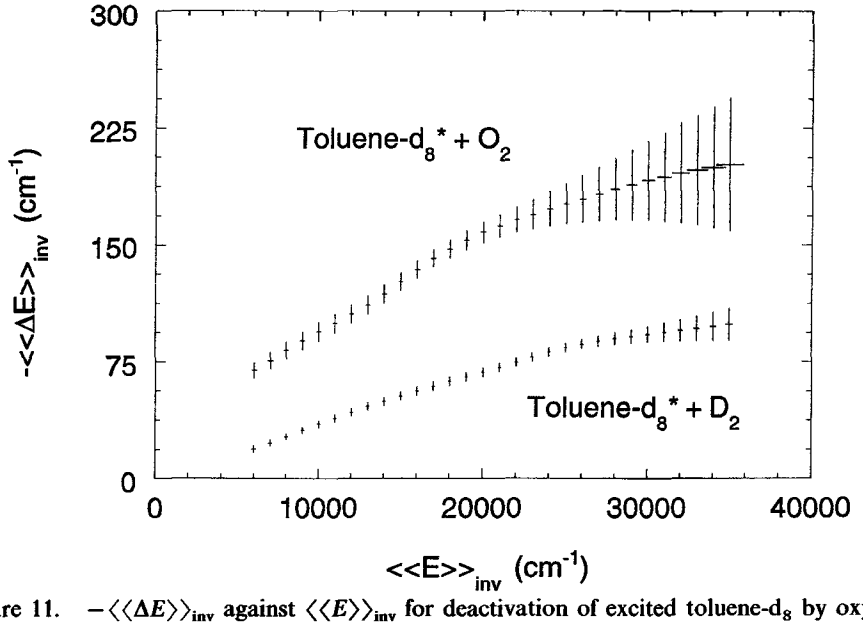

Figure 11. $-\langle\langle \Delta E \rangle\rangle_{inv}$ against $\langle\langle E \rangle\rangle_{inv}$ for deactivation of excited toluene-d_8 by oxygen (Toselli and Barker 1992).

vibrational energy is nearly linear, but at higher energies, many of the plots tend to level off and, in some cases, the magnitude of $\langle\langle\Delta E\rangle\rangle_{\text{inv}}$ even decreases at the highest energies. The reasons for this behaviour are still a mystery, although we offer some speculations below.

5.2. $\langle\Delta E\rangle_d$ *from* $\langle\langle\Delta E\rangle\rangle_{inv}$ *data*

For master equation calculations, weak-collider unimolecular reaction calculations, and other numerical simulations of chemical systems where energy transfer plays a role, it is often most convenient to use energy transfer data in the form of $\langle\Delta E(E)\rangle_d$, the microcanonical average energy lost in deactivation collisions as a function of the microcanonical energy E. Since the IRF and UVA techniques give results in terms of bulk averages over both up- and down-steps and over a population energy distribution, further analysis is needed to extract $\langle\Delta E\rangle_d$.

In this Section, we describe an efficient method for obtaining estimates of $\langle\Delta E(E)\rangle_d$ (exponential model for $P(E', E)$) directly from $\langle\langle\Delta E\rangle\rangle_{\text{inv}}$ data sets, eliminating the need for the time-consuming master equations simulations (Toselli *et al.* 1991).

An approximate relationship between $\langle\Delta E\rangle_d$ and $\langle\Delta E\rangle$ (average over up- and down-steps) was derived previously (Barker and Golden 1984), based on detailed balance between up- and down-steps, the exponential model for down-steps, and the Whitten and Rabinovitch (1964) approximation for densities of states. The unnormalized exponential model for down-steps is given by

$$P(E', E) = \exp[-(E - E')/\alpha] \qquad 0 \leqslant E' \leqslant E, \tag{11}$$

where α is a parameter. For this model, $\langle\Delta E\rangle_d$ is given by

$$\langle\Delta E\rangle_{\text{d}} = \frac{\int_0^E (E - E')P(E', E)\,\text{d}E'}{\int_0^E P(E', E)\,\text{d}E'} = \frac{\alpha - (E - \alpha)\exp(-E/\alpha)}{[1 - \exp(-E/\alpha)]}. \tag{12}$$

An approximate relationship between $\langle\Delta E\rangle$ and α is

$$\langle\Delta E\rangle = C^{-1} - \alpha, \tag{13}$$

$$C = \alpha^{-1} + (kT)^{-1} - B. \tag{14}$$

The factor $B = \text{d}\{\ln[\rho(E)]\}/\text{d}E$ is based on the Whitten–Rabinovitch (1964) approximation for the density of rovibrational states (Forst 1973):

$$B = \frac{s - 1 + r/2}{E + a(E)E_z}, \tag{15}$$

where s is the number of vibrations, r is the number of rotations, E_z is the zero-point energy, and $a(E)$ is the Whitten–Rabinovitch parameter. Equation (13) for $\langle\Delta E\rangle$ has been shown to give results in good agreement with values obtained by numerical integration (carried out with exact densities of states) both at low temperatures, where $\langle\Delta E\rangle$ is less than zero, and at high temperatures, where $\langle\Delta E\rangle$ can be greater than zero (Barker and Golden 1984).

A simple approximate relationship between $\langle\Delta E\rangle_d$ and $\langle\Delta E\rangle$ is obtained from the preceding equations by assuming $\alpha = \langle\Delta E\rangle_d$; this relationship is numerically accurate to $\pm 10\%$, except at energies less than a few times α. Although α may be energy dependent, the dependence on energy is found experimentally to be weak and it does

Table 2. Collider gas data for the deactivation of benzene derivatives.

Collider	σ^a_{LJ} (Å)	ε/K^a (K)	$10^{10}k_{LJ}$ ($cm^3\,s^{-1}$)	$-\langle\langle\Delta E\rangle\rangle^{b,c}_{inv}$ (cm^{-1})	$\langle\Delta E\rangle^d_d$ C_1 (cm^{-1})	C_2	10^7C_3 ($1/cm^{-1}$)
Benzene-d_0[f]							
A_6H_6	5·27	440	6·5	869 ± 17	41·5	0·0539	−4·58
^3He[e]	2·551	10·22	5·37	26 ± 1	20·1	0·00367	−0·019
^4He	2·551	10·22	6·16	23 ± 1	20·7	0·00421	−0·453
Ne	2·82	32·8	3·75	20 ± 1	18·7	0·00442	−0·777
Ar	3·542	93·3	4·07	30 ± 3	17·8	0·00582	−0·991
Kr	3·655	178·9	3·8	34 ± 1	28·4	0·00521	−0·738
Xe	4·047	231	3·95	36 ± 2	28·0	0·00594	−0·986
H_2	2·827	59·7	11·77	66 ± 3	34·2	0·00779	−0·982
D_2	2·73	69	8·42	45 ± 2	29·8	0·00716	−1·27
N_2	3·798	71·4	4·67	34 ± 2	27·6	0·00526	−0·778
O_2	3·467	106·7	4·42	37 ± 2	19·5	0·00625	−0·938
CO	3·69	91·7	4·75	37 ± 4	25·9	0·00591	−0·902
CO_2	3·941	195·2	4·93	208 ± 4	47·7	0·0202	−3·11
H_2O	2·641	809·1	6·94	373 ± 36	84·4	0·0277	−3·51
NH_3	2·9	558·3	6·9	348 ± 78	2·85	0·0232	−0·957
CH_4	3·758	148·6	6·54	163 ± 17	15·1	0·0173	−2·34
SF_6	5·128	222·1	4·79	538 ± 49	48·2	0·0398	−0·482
c-C_3H_6	4·807	248·9	6·28	635 ± 120	27·3	0·0616	−12·05
C_3H_6	4·78	271	6·36	424 ± 56	31·9	0·0418	−7·57
n-C_4H_{10}	4·687	531·4	6·56	615 ± 50	32·9	0·0535	−9·044
Benzene-d_6							
C_6D_6	5·27	440	6·27	576 ± 6	61·3	0·0452	−6·60
H_2	2·83	60	11·80	61 ± 1	38·0	0·0071	−0·92
D_2	2·73	69	8·43	46 ± 1	28·6	0·0055	−0·53
Toluene-d_0							
C_7H_8	5·92	410	7·32	867 ± 18	46·2	0·0538	−4·57
^3He[e]	2·55	10	8·21	60 ± 1	24·7	0·00753	0·865
^4He[e]	2·55	10	7·14	62 ± 1	28·6	0·00784	−1·00
Ne	2·82	32	4·26	77 ± 2	32·4	0·00984	−1·47
Ar	3·47	114	4·62	112 ± 3	36·1	0·00898	0·0323
Kr	3·66	178	4·15	110 ± 4	36·1	0·00985	−0·769
Xe	4·05	230	4·25	124 ± 6	44·1	0·00954	−0·0406
H_2	2·83	60	13·57	89 ± 3	29·1	0·01066	−1·49
D_2	2·73	69	9·69	103 ± 2	38·7	0·01164	−1·69
N_2	3·74	82	5·27	139 ± 4	39·3	0·0159	−2·63
O_2	3·84	103	4·93	151 ± 3	35·4	0·0142	−1·63
CO	3·70	105	5·44	163 ± 3	34·8	0·0144	−1·47
CO_2	3·94	201	5·46	245 ± 6	37·4	0·0230	−3·33
H_2O	2·71	506	7·13	364 ± 13	52·1	0·0323	−5·05
D_2O	2·71	506	6·82	293 ± 8	70·4	0·01797	−0·691
CH_4	3·79	153	7·43	225 ± 6	47·1	0·0197	−2·54
NH_3	2·90	558	7·80	285 ± 10	48·6	0·0213	−1·94
SF_6	5·20	212	5·09	368 ± 4	46·9	0·0292	−3·50
c-C_3H_6	4·63	299	6·86	576 ± 12	22·6	0·0473	−7·01
C_3H_6	4·78	271	6·92	487 ± 12	38·7	0·0333	−0·307
n-C_4H_{10}	5·40	307	7·15	619 ± 18	57·2	0·0403	−3·51

Table 2. (*continued*)

	σ_{LJ}^{a} (Å)	ε/K^{a} (K)	$10^{10}k_{LJ}$ ($cm^3\,s^{-1}$)	$-\langle\langle\Delta E\rangle\rangle_{inv}^{b,c}$ (cm^{-1})	$\langle\Delta E\rangle_d^d$ C_1 (cm^{-1})	C_2	10^7C_3 ($1/cm^{-1}$)
Toluene-d_8							
C_7D_8	5·92	410	7·02	747±13	30·5	0·0611	−9·48
$^3He^e$	2·55	10	8·0	53±2	41·8	0·0061	−0·74
^4He	2·55	10	7·13	60±1	37·4	0·0080	−1·25
Ne	2·82	32	4·23	87±3	46·3	0·0103	−1·66
Ar	3·47	114	4·48	126±3	54·1	0·0135	−2·17
Kr	3·66	178	4·07	126±4	49·6	0·0129	−1·88
Xe	4·05	230	4·15	138±5	55·1	0·0129	−1·68
H_2	2·83	60	13·56	82±3	43·2	0·0092	−1·26
D_2	2·73	69	9·67	81±3	39·2	0·0091	−1·19
N_2	3·74	82	5·22	121±4	32·1	0·0111	−0·97
O_2	3·48	103	4·88	173±11	114·8	0·0122	−1·62
CO	3·70	105	5·39	133±5	32·0	0·0130	−1·49
H_2O	2·71	506	7·08	387±14	56·3	0·0237	−1·18
D_2O	2·71	506	6·77	378±25	35·5	0·0225	−0·49
CH_4	3·79	153	7·38	199±6	55·6	0·0179	−2·47
NH_3	2·90	558	7·75	350±12	−1·7	0·0327	−4·86
SF_6	5·20	212	4·96	337±12	46·4	0·0246	−2·28
c-C_3H_6	4·63	299	6·78	461±18	46·0	0·0281	−1·51
C_3H_6	4·78	271	6·83	441±15	86·4	0·0317	−3·90
n-C_4H_{10}	5·40	307	7·04	530±20	−3·3	0·0394	−4·18

[a] Lennard–Jones parameters (Hippler and Troe 1989, Hippler *et al.* 1989). When parameters for deuterated species are not available, the parameters for the corresponding normal isotopomer were used.
[b] Uncertainties are $\pm 2\sigma$ statistical errors; possible systematic errors are not included.
[c] Evaluated at $\langle\langle E\rangle\rangle_{inv} = 24\,000\,cm^{-1}$.
[d] $\langle\Delta E(E)\rangle_d = C_1 + C_2E + C_3E^2$.
[e] Re-analysed data from Toselli and Barker (1990).
[f] Re-analysed data from Yerram *et al.* (1990).

not significantly affect the equations above, where energy dependence was not considered. To obtain $\langle\Delta E(E)\rangle_d$ from $\langle\langle\Delta E\rangle\rangle_{inv}$ against $\langle\langle E\rangle\rangle_{inv}$ data sets, we first neglect the effect of the bulk population distribution and assume $E \approx \langle\langle E\rangle\rangle_{inv}$ and then identify $\langle\Delta E\rangle$ with $\langle\langle\Delta E\rangle\rangle_{inv}$ (Toselli *et al.* 1991). The estimated $\langle\Delta E(E)\rangle_d$ is obtained by expanding it as a power series with coefficients that are adjusted by least squares to give agreement between $\langle\Delta E\rangle$ calculated from the above equations and the experimental $\langle\langle\Delta E\rangle\rangle_{inv}$ values. Excellent fits to the experimental data are obtained using $\langle\Delta E(E)\rangle_d = C_1 + C_2E + C_3E^2$; use of a higher-order polynomial does not produce better least-squares fits to the data. The fitted values for the coefficients are collected in table 2 and they provide useful functional forms for $\langle\Delta E(E)\rangle_d$. They also may be used with the above equations to reproduce accurate numerical values for all the $\langle\langle\Delta E\rangle\rangle_{inv}$ against $\langle\langle E\rangle\rangle_{inv}$ data sets over the range of energies from 5000 cm^{-1} to 35 000 cm^{-1} (40 000 cm^{-1} for pure aromatic colliders). For convenience, the Whitten–Rabinovitch parameters used in this analysis are summarized in table 3.

Master equation simulations were carried out to determine whether the approximate expressions for $\langle\Delta E(E)\rangle_d$ obtained above are useful for quantitative calculations

Table 3. Whitten–Rabinovitch parameters†.

Species	Zero-point energy (cm^{-1})	β	Vibrational degrees of freedom (s)	Rotor degrees of freedom (r)
Benzene-d_6	21399·35	1·3281	30	0
Benzene-d_6	17290·5	1·2616	30	0
Toluene-d_0	27109	1·3644	38	1
Toluene-d_8	21708	1·3010	38	1

† Defined in Whitten and Rabinovitch (1964).

(Toselli *et al.* 1991). Specifically, the IRF experiments were simulated using the stochastic master equation implementation described elsewhere (Barker 1983, Barker and Golden 1984, Shi and Barker 1990), assuming an exponential model and energy-dependent $\langle \Delta E(E) \rangle_d$ from table 2. The calculated IRF decay curves were inverted to energy decays according to the procedure described above and $\langle\langle \Delta E \rangle\rangle_{inv}$ against $\langle\langle E \rangle\rangle_{inv}$ data sets were generated from the derivatives of polynomial least squares fits of $\langle\langle E \rangle\rangle_{inv}$ as a function of the number of collisions. The results show agreement within ~5–10%. Further refinements are not justified at this time, because the actual functional form of $P(E', E)$ is not yet known and it is not likely to be a simple exponential. However, it is noteworthy that $\langle \Delta E(E) \rangle$ data for most collider gases investigated so far have a tendency to roll off at higher energy, as is reflected in the plots of $\langle\langle \Delta E \rangle\rangle_{inv}$ against $\langle\langle E \rangle\rangle_{inv}$.

6. Vibration-to-vibration (V–V) energy transfer

Spontaneous infrared emission from the product of an energy transfer collision can be used to investigate V–V energy transfer (Barker *et al.* 1982, Rossi *et al.* 1983, Barker 1984, Toselli and Barker 1991). The magnitude of this process provides some insight into the mechanisms important in large molecule energy transfer systems.

6.1. *Experimental techniques*

IRF is viewed through a quartz side window (to monitor the C–H emission near 3·3 μm) or through a CaF_2 side window (to monitor the C–D emission and/or the CO_2(001) spontaneous emission near 4·3 μm) with a detector and appropriate interference filters.

In the experiments designed to measure the deactivation of the excited parent by CO_2, the pressure of parent was held constant at 10 mtorr and the CO_2 pressure was varied from 50 to 300 mtorr. The experiments designed to measure the production of CO_2^* and its subsequent deactivation were performed under static bulb conditions in mixtures containing 30 to 70 mtorr of benzene or its derivatives and 10 and 20 mtorr of CO_2. The CO_2 pressures were kept low to avoid self-absorption by the strongly absorbing CO_2 in the ~3 cm pathlength between the emission volume and the window of the cell (Huddleston *et al.* 1982).

The laser fluence was ~25 mJ cm^{-2} per shot, so that approximately 0·5% of the molecules in the laser beam were excited. It was shown in earlier experiments that the quantum yield for photodissociation of these aromatics at 248 nm is of the order of 5%, but this does not cause problems, because the fragments carry little excitation energy and do not emit significantly, as explained above.

6.2. *Formation of* CO_2^*

The rate of production of excited CO_2 was monitored by observing the spontaneous emission of the asymmetric stretch mode (v_3) isolated with a band-pass filter near 4·3 μm. The actual states of the excited CO_2 cannot be identified from these measurements, except that the 4·3 μm band is associated with $\Delta v_3 = -1$. Thus the excited species is designated CO_2^*. There is some evidence in the azulene + CO_2 system that two or more vibrational modes of CO_2 can be excited simultaneously, but there is no direct evidence that more than one quantum resides in v_3, which has a relatively high vibrational frequency (Rossi *et al.* 1983). Thus, the CO_2^* probably can be identified with $CO_2(v_1\, v_2\, 1)$, where $v_1, v_2 \geqslant 0$.

In all of the experiments carried out with benzene derivatives and aimed at measuring the production of CO_2^*, the CO_2 pressure was kept low for two reasons: (1) to avoid complications due to self absorption of the 4·3 μm IRF by CO_2 (Huddleston *et al.* 1982), and (2) to allow the collisional deactivation of excited parent (P^*) to be dominated by $P^* + P$ collisions, rather than $P^* + CO_2$ collisions.

The CO_2^* emission was isolated with an interference filter that also transmitted some of the emission from the C–D stretching vibrations. In the case of the benzene-d_0 or toluene-d_0, the total emission measured through the interference filter was mostly due to CO_2^*, although there was a small IRF intensity due to the emission of the excited parent. Typical signals observed near 4·3 μm for benzene–CO_2 and toluene–CO_2 are shown in figure 12. The results obtained with the two excited non-deuterated species are similar, although the yield of CO_2^* is not as great for toluene-d_0. In the case of the deuterated species, the analysis of the IRF signal is complicated due to the presence of strong emission from the C–D stretching modes near $\sim 2300\,cm^{-1}$ and little quantitative information on production of CO_2^* could be obtained (Toselli and Barker 1991).

Each of the IRF intensity decay curves in figure 12 is characterized by a detector-limited rapid rise, often followed by a more gradual rise to a maximum, followed by a slower decay. For the deuterated compounds, a maximum is not observed and the final decay is on a very long time-scale. The general features of this behaviour can be explained as the sum of contributions at 4·3 μm from excited parent and from CO_2^*. For convenience in the analysis, the IRF signals were fitted to the following empirical function:

$$\langle\langle I(t)\rangle\rangle = I_A[1 - \exp(-k_a t)]\exp(-k_b t) + I_P \exp(-k_c t). \tag{16}$$

6.3. *Rate of deactivation of* CO_2^* *by the unexcited parent*

The CO_2^* is deactivated only very slowly by unexcited CO_2 (Chou *et al.* 1989), and so the long decay is due to diffusion and to collisional deactivation by the parent molecule (figure 12). In a series of experiments, the pressure of the aromatic was varied between 30 to 70 mtorr for two pressures of CO_2 (10 and 20 mTorr). The 4·3 μm IRF signal (due mostly to CO_2^* emission for non-deuterated systems, and to both the C–D stretches of the aromatic and CO_2^* for the deuterated systems) was fitted by least-squares to equation (16). The IRF was observed using a long time-scale and the least-squares fits included only the data corresponding to the time subsequent to CO_2^* formation.

In collisions with benzene-d_0 and with toluene-d_0, it was found that the observed CO_2^* fluorescence decays are fitted well by a single exponential and the first order decay rate constants were found to be nearly proportional to the pressure of the aromatic (figure 13). In collisions with the deuterated aromatics, the CO_2^* fluorescence decays

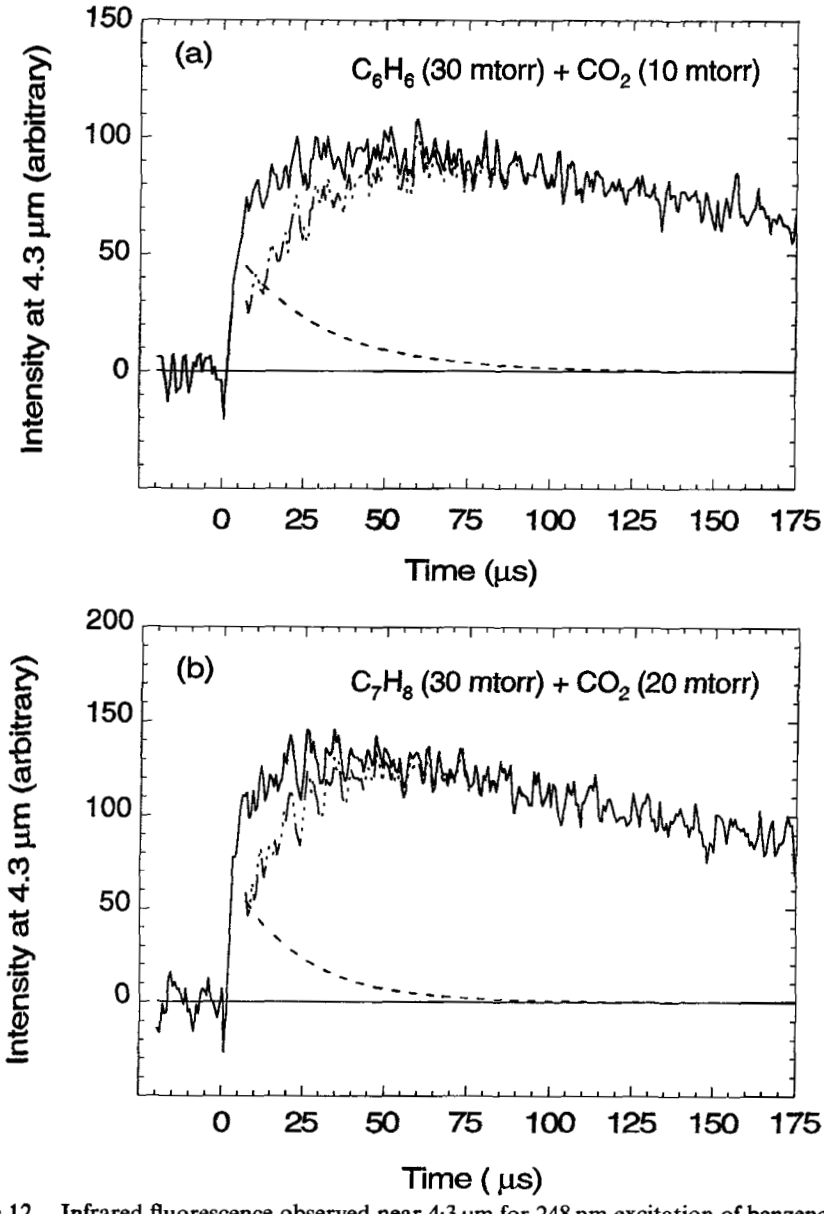

Figure 12. Infrared fluorescence observed near 4·3 μm for 248 nm excitation of benzene-d_0 or toluene-d_0 mixed with CO_2 (Toselli and Barker 1991). The solid line represents the actual measured intensity and the dashed lines show the contribution to the total intensity from $CO_2^{\ddagger}$ and excited parent emissions.

were also well-described by a single exponential function, but they were much slower than observed with the non-deuterated species. Furthermore, the first-order decay rate constants actually *decrease* with increasing [*P*] in a manner which is consistent with diffusion from the field of view of the detector, or to the walls where deactivation can occur (figure 13). The difference in behaviour between the deuterated and the non-deuterated molecules may be due to reversible near-resonant energy transfer between

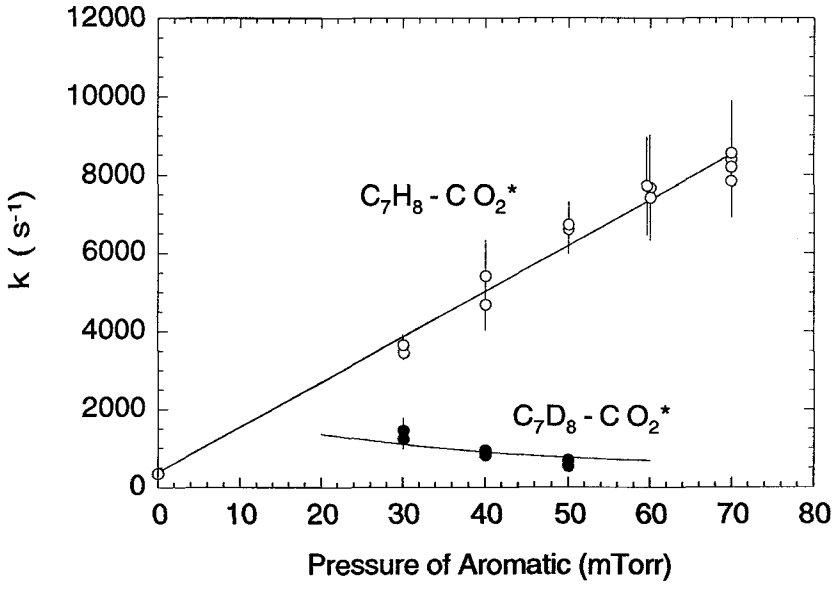

Figure 13. The deactivation of CO_2^* by unexcited toluene or toluene-d_8 (Toselli and Barker 1991). The results for toluene-d_8 are almost completely controlled by diffusion (see text for details).

the ν_3 mode of CO_2 (2349 cm^{-1}) and the C–D stretching modes ($\sim$2300 cm^{-1}) in the deuterated aromatics. In the non-deuterated cases, the observed fluorescence decay corresponds to deactivation of CO_2^* by collisions with parent molecules.

6.4. *Probability of CO_2^* formation*

The total yield of CO_2^* produced was determined relative to the initial concentration of excited parent in the following way. The total yield of CO_2^* is proportional to its fluorescence intensity near $h\nu_{CO_2}=2349\,cm^{-1}$ at very long times, neglecting collisional deactivation of the CO_2^* (I_A from equation (16)). Similarly, the initial concentration of excited parent, $[P^{**}]_0$, is proportional to the initial intensity I_P^* at $h\nu_P$ (the fundamental of the C–H or C–D stretch modes) as expressed by equation (7). Equation (7) can be re-written as follows for the C–H stretch modes:

$$I_P^* = [P^{**}]_0 \frac{h\nu_P A_P}{\rho_s(E_0)} \sum_{v=1}^{v_{max}} v\rho_{s-1}(E_0 - vh\nu_P), \tag{17}$$

where $E_0 \approx 40\,500\,cm^{-1}$ (the initial excitation energy of the aromatic), $h\nu_P$ is the emission band frequency of the parent, A_P is the Einstein coefficient of the whole band for parent, and A_{CO_2} is the Einstein coefficient for CO_2 emission at 2349 cm^{-1}. Thus, the total concentration of CO_2^* produced, relative to the initial concentration of excited parent is

$$\frac{[CO_2^*]_\infty}{[P^{**}]_0} = \frac{I_A}{I_P^*} \frac{h\nu_P A_P}{h\nu_{CO_2} A_{CO_2}} \frac{1}{\rho_s(E_0)} \sum_{v=1}^{v_{max}} v\rho_{s-1}(E_0 - vh\nu_P). \tag{18}$$

In equation (16), the term $I_A[1-\exp(-k_a t)]$ is proportional to the time-dependent concentration of CO_2^* (neglecting its deactivation), which asymptotically approaches $[CO_2]_\infty$. Therefore, the rate of production of CO_2^* is given by the following expression:

$$\frac{d}{dt}[CO_2^*] = [CO_2^*]_\infty k_a \exp(-k_a t). \tag{19}$$

We can also write the rate of production as a bimolecular reaction between the excited aromatic and CO_2, with the rate constant set equal to the collision rate constant (k_{LJ}^c) and multiplied by the probability $Q(t)$ that V–V energy transfer will take place. Recognizing that the total concentration of excited aromatic does not change (only the average energy changes), the rate of production of excited CO_2 can be written:

$$\frac{d}{dt}[CO_2^*] = Q(t) k_{LJ}^c [CO_2][P^{**}]_0, \tag{20}$$

where $[P^{**}]_0$ is the concentration of excited aromatic produced in the laser pulse. Equations (19) and (20) are combined to obtain the probability for V–V transfer as a function of time:

$$Q(t) = \frac{[CO_2^*]_\infty k_a \exp(-k_a t)}{[P^{**}]_0 k_{LJ}^c [CO_2]}, \tag{21}$$

This expression is evaluated by using equation (18) to determine the ratio $[CO_2^*]_\infty/[P^{**}]_0$. During the time when the CO_2^* is building up, the energy in the excited parent is decaying away. Thus, at any instant of time, $Q(t)$ is associated with the excitation energy $\langle\langle E\rangle\rangle_m$ (the subscript denotes the mixing ratio), thus the probability can be expressed as $Q(E)$, a function of excitation energy. Note that the energy-dependence of $Q(E)$ does not depend in any strong way on the particular gas mixture composition or total pressure, which mainly affect the time-dependences of $Q(t)$ and $\langle\langle E\rangle\rangle_m$.

The probabilities obtained from the experimental data using equation (21) are shown in figure 14 as closely spaced vertical bars of $\pm 1\sigma$ statistical uncertainty. The detailed shapes of the $Q(E)$ curves depend both on the assumed form of empirical equation (16) (which fits the data well for the non-deuterated species and not as well for the deuterated species) and on the densities of states of the excited parent, according to equation (18). In all cases investigated, the probabilities are small, in agreement with other studies, indicating that V–V energy transfer from highly excited molecules is not very efficient when the receptor is a high frequency vibration, such as the asymmetric stretch in CO_2.

The $Q(E)$ curves for the non-deuterated species are approximately linear and each may have a small intercept on the energy axis near $\langle\langle E\rangle\rangle \geqslant 2349\ cm^{-1}$, which is the energy of the $CO_2(001)$ state. For the deuterated species, interference from the C–D stretch mode emission introduces large uncertainties in the curve-fitting which are not reflected by the $\pm 1\sigma$ statistical error bars. We have little confidence in the detailed shapes of the $Q(E)$ curves for the deuterated species, although the magnitudes are similar to those for the non-deuterated species.

The energy-dependent $Q(E)$ can be used to calculate the ratio $[CO_2^*]_\infty/[P^{**}]_0$ for any mixture of CO_2 and parent, and when $F_c = 1$, $\langle\langle \Delta E\rangle\rangle_m$ corresponds to pure CO_2 and the calculated $[CO_2^*]_\infty/[P^{**}]_0$ ratio corresponds to infinite dilution. For benzene-d_0 and toluene-d_0, the ratios at infinite dilution were found to be $0{\cdot}078 \pm 0{\cdot}026$ and

$0{\cdot}052 \pm 0{\cdot}017$, respectively, where the uncertainties are estimated to be $\pm 33\%$. These results cannot be compared directly with those obtained by Sedlacek *et al.* (1991), because those authors obtained their results for a mixture consisting of 20 mtorr of benzene diluted in 80 mtorr of CO_2, where they found $[CO_2^*]_\infty/[P^{**}]_0 = 0{\cdot}032 \pm 0{\cdot}011$. From the present energy transfer data and for the specific conditions of their experiments, it is calculated that $[CO_2^*]_\infty/[P^{**}]_0 = 0{\cdot}032 \pm 0{\cdot}011$ for 20 mtorr of benzene diluted in 80 mtorr of CO_2, in excellent agreement with the experimental data of Sedlacek *et al.* (1991) (the exact numerical agreement is coincidental).

6.5. *Model for the probability of CO_2^* formation*

To explain the observed magnitude of the probabilities and to predict the amount of energy transferred to the other vibrational modes of CO_2, we derived a simple model based on long-range dipole–dipole interactions. The derivation is similar to that for Förster energy transfer (Yardley 1980), but it also incorporates three other concepts: (1) natural broadening of the upper state due to its short lifetime with respect to intramolecular vibrational redistribution (IVR), (2) statistical distribution of vibrational energy among the normal modes, and (3) straight line trajectories, because the dipole–dipole forces are effective over long distances. The only adjustable parameter in the model is the IVR time constant, τ_D, since all other parameters are obtained from infrared spectra of the aromatics.

Mahan (1967) was the first to suggest that long-range electrostatic dipole–dipole interactions could be important for inducing near resonant V–V energy transfer. Only a few years earlier, Förster (1965) described electronic energy transfer involving species in viscous solvents in terms of interactions between the transition dipoles of the two species, according to Fermi's golden rule. In our model, we adapted these ideas and assumed that the long-range dipole–dipole interactions can be described satisfactorily by straight line trajectories and that the rate of change of the interaction is sufficiently slow so that Fermi's golden rule can be applied to calculate the transition probability. This probability is an opacity function which can be used to calculate the cross-section for V–V energy transfer by invoking the Sharma–Brau cut-off (Yardley 1980) at the Lennard–Jones σ_{LJ}. By integrating over the Maxwell–Boltzmann speed distribution, the thermal rate constant is obtained:

$$k_c = \frac{5\pi^2 K(\Delta\omega)}{8\sigma_{LJ}^3}, \tag{22}$$

where $K(\Delta\omega)$ is a constant which depends on the overlap of the emission band of the 'donor' and the absorption band of the 'acceptor' and that overlap depends on $\Delta\omega$, the frequency difference between the two bands.

Equation (22) was derived as if two isolated dipoles were interacting. In the present system, a CO_2 acceptor dipole interacts with a large molecule, which contains many dipoles and whose vibrational energy is presumed to be rapidly distributed among all vibrational degrees of freedom due to rapid IVR. The coupling associated with IVR broadens each vibrational state and it can be characterized by a characteristic lifetime, which we assume is identified with τ_i in the linewidth function. For the large molecule (energy donor), τ_D is expected to be of the order of 0·1–10 ps, values typical of IVR time constants (Smalley 1983). For the CO_2 vibrational states, which are not significantly coupled, τ_A is just the natural life-time (energy acceptor), which is very long. Thus, the spectral linewidth of the acceptor absorption band, $g_A(\Delta\omega)$, can be treated as a delta function, while the emission band linewidth, $g_D(\Delta\omega)$, of the donor is a Lorentzian with

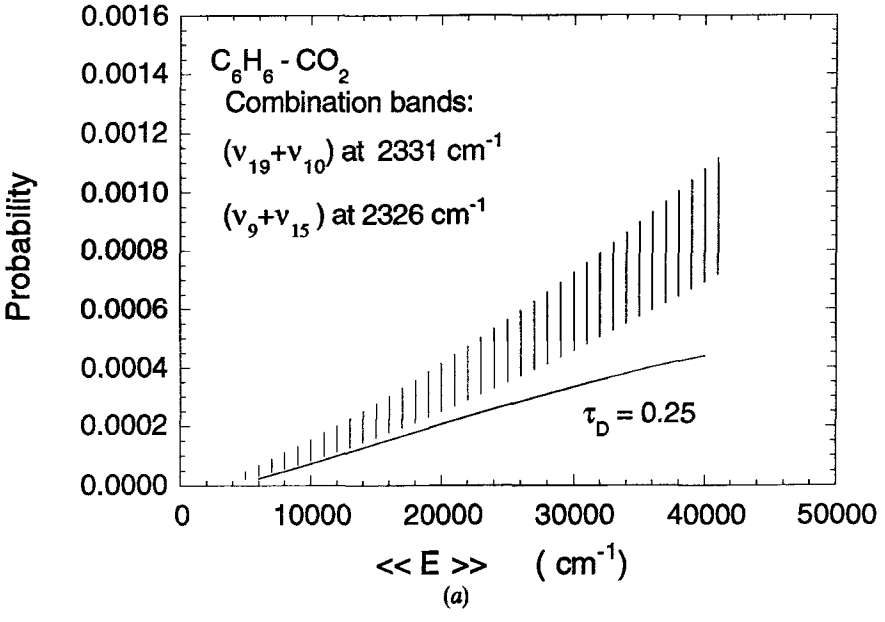

(*a*)

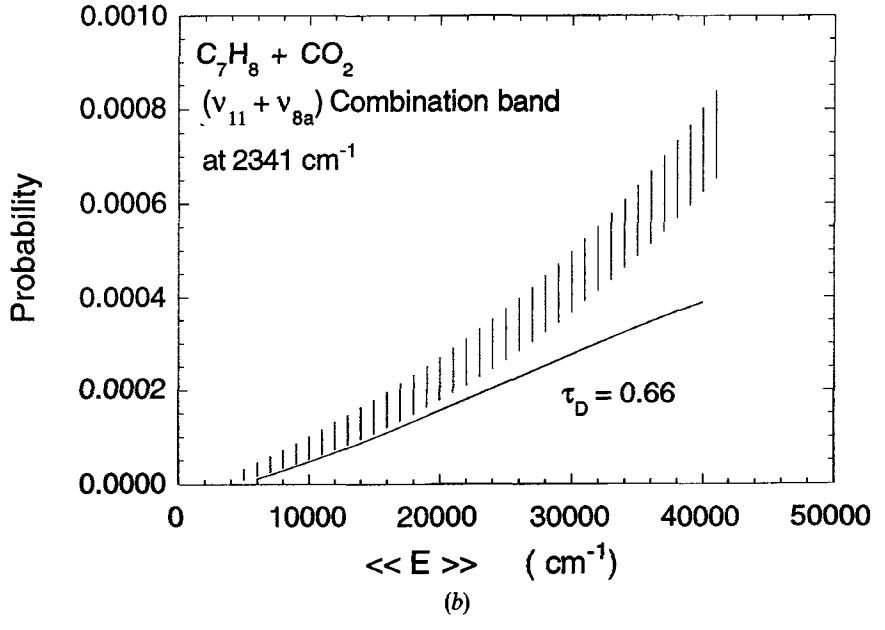

(*b*)

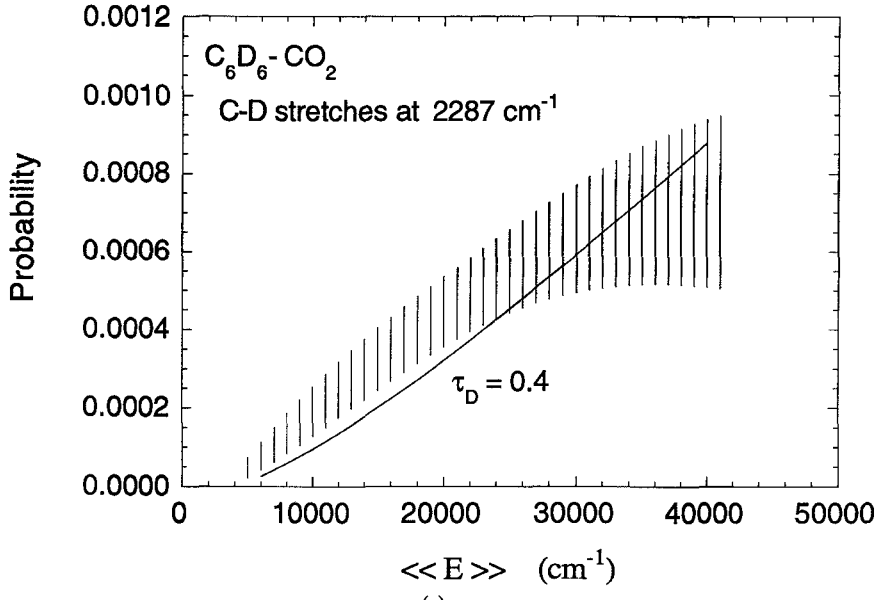

(*c*)

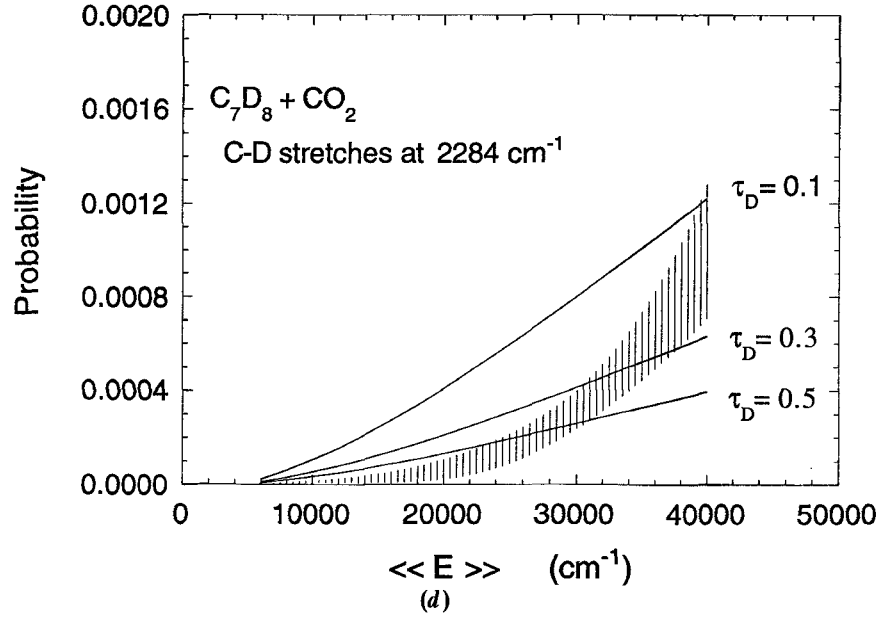

(*d*)

Figure 14. Experimental and calculated probabilities 'per collision' of CO_2^* formation (Toselli and Barker 1991). Also indicated are the infrared transitions in the excited polyatomic that make the major contributions to the calculated probabilities.

linewidth related to τ_D. With these assumptions, the spectral overlap is just $g_D(\Delta\omega)$ and $K(\Delta\omega)$ has a Lorentzian dependence on frequency difference.

The redistribution of energy due to IVR requires that equation (22) be multiplied by the probability that the donor mode in the parent contains one or more quanta ($v_D \geqslant 1$). Moreover, the rate constant is proportional to v_D, when harmonic oscillator wavefunctions are used to evaluate the matrix elements for fundamentals (slight revisions to the matrix elements are needed for combination bands (Peyret and Flaud 1985)). If we assume that the energy distribution among the modes in a single molecule is 'frozen' just before the collision takes place, the probability of finding v_D quanta in the donor mode can be determined from statistical theory in just the same way as equation (7) is derived. Both the scaling with v_D and the statistical factor are included in the following expression for k_c for energy transfer from the vibrational fundamentals of large molecule donors (the expression must be modified slightly for combination bands):

$$k_c = \frac{5\pi^2 K(\Delta\omega)}{8\sigma_{LJ}^3} \frac{1}{\rho_s(E)} \sum_{v_D=1}^{v_{max}} v_D \rho_{s-1}(E - v_D h\nu_D), \tag{23a}$$

where

$$K(\Delta\omega) = \frac{2\pi\mu_D^2\mu_A^2}{(h/2\pi)^2} \kappa^2 g_D(\Delta\omega). \tag{23b}$$

Here, μ_D and μ_A are the transition dipoles of the donor and acceptor, respectively, κ is a geometric factor, which is taken to be unity, and $g_D(\Delta\omega)$ is the lineshape function describing the emission band of the donor.

For comparison with the experimental data for $Q(E)$, which is expressed on a per-collision basis, we define a calculated probability per collision $Q_c(E)$:

$$Q_c(E) = \frac{k_c}{k_{LJ}}. \tag{24}$$

For a fixed value of τ_D, the probability $Q_c(E)$ decreases very dramatically with the frequency mismatch, due to the linewidth function, and the matrix elements are only significant when the energy difference is less than $\sim 100\,\text{cm}^{-1}$: near-resonance is required.

The experimental probabilities and those calculated according to this model are presented in figure 14. It was found that $Q_c(E)$ goes through a maximum as τ_D is varied, and the best fit for the non-deuterated molecules is obtained for the value of τ_D which maximizes $Q_c(E)$. As shown in figure 14, the agreement between $Q(E)$ and $Q_c(E)$ is good, although $Q_c(E)$ is near the maximum value that this simple model can predict for non-deuterated species. There are many assumptions incorporated in the model that may affect the magnitude of $Q_c(E)$. Despite the limitations of the simple model, the major conclusion is that dipole–dipole interactions appear to explain the V–V energy transfer process. When trajectory calculations (Bruehl and Schatz 1988a, b, Lim and Gilbert 1990) and more sophisticated theories (see Gilbert and Smith (1990), chap. 5) are applied to these systems, it will be very important to include dipole–dipole interactions.

7. Discussion of large molecule energy transfer mechanisms

Our work is aimed at understanding the mechanisms of large molecule energy transfer and providing a data base for comparisons with theory. One would expect that the same physical properties that are important for small molecules would also be

present in large molecule energy transfer. Thus it is not surprising that dipole–dipole interactions can explain the extent of V–V energy transfer, as described above, and they must be considered in future theoretical calculations.

In our present view, the collisional deactivation of large molecules can be described with the following components:

(1) V–T and V–R energy transfers take place with all colliders, probably due to the short-range repulsive interactions invoked in the biased random walk model (although a classical mechanics description is not quantitatively valid);
(2) V–V energy transfer can take place by long-range dipole–dipole interactions, and thus resonance may play a role;
(3) if the collider gas has a permanent dipole moment, it is likely that the permanent dipole can interact with the vibrating dipoles of the excited molecule and therefore V–R energy transfer will be enhanced;
(4) if low-lying excited electronic states are present, they may enhance energy transfer rates very substantially (Toselli *et al.* 1990).

These components must be combined with properties of the large molecules involved: very large densities of states and statistical distribution of energy among the vibrational modes. Some of the rationales for including these components are summarized below, but first, possible quantum effects are discussed.

7.1. *Possible quantum effects*

Quantum effects were invoked by Gilbert and Zare (1990) as one possible explanation for uneven performance of classical trajectory calculations (Lim and Gilbert 1990) in describing deactivation of highly vibrationally excited azulene by the rare gases. Trajectory calculations for deactivation by the heavier rare gases agreed well with experimental data, while those for the lighter rare gases showed large discrepancies with experiment. Two possible explanations were proposed: (1) the potential energy surfaces for the azulene + lighter rare gases are in error, and (2) quantum effects are important for the lighter systems, but not for the heavier ones. The proposed quantum effects were thought to arise from two possible sources: (1) zero-point energy, which is conserved in quantum systems, but can be transferred in classical trajectory calculations, and (2) a dynamical quantum effect due to interferences among matter waves with small deflection angles at large impact parameters (these same interferences are responsible for the finite quantum total elastic cross-sections, while the corresponding classical cross sections are infinite).

Gilbert and Zare (1990) proposed a test for the dynamical quantum effect: that deactivation of excited species by ^{3}He and ^{4}He be investigated. These colliders have a relatively large mass difference, but the potential energy surface is unaffected, and the average energy transferred should be affected significantly if the dynamical quantum effect is important. Experiments carried out in this laboratory (Toselli and Barker 1990) show that the two helium isotopes have nearly identical energy transfer parameters, as presented in table 2 and in figure 15. The dynamical quantum effect is not important, if Gilbert and Zare are correct in their speculation that the ^{3}He/^{4}He mass difference will produce a large difference in energy transfer parameters.

However, quantum effects may still be important in defining the differences between quantum systems and classical trajectory calculations on energy transfer: quantum and classical population statistics are significantly different (Toselli and Barker 1990, 1992). In a classical system of coupled oscillators, the energy is randomized so that the average

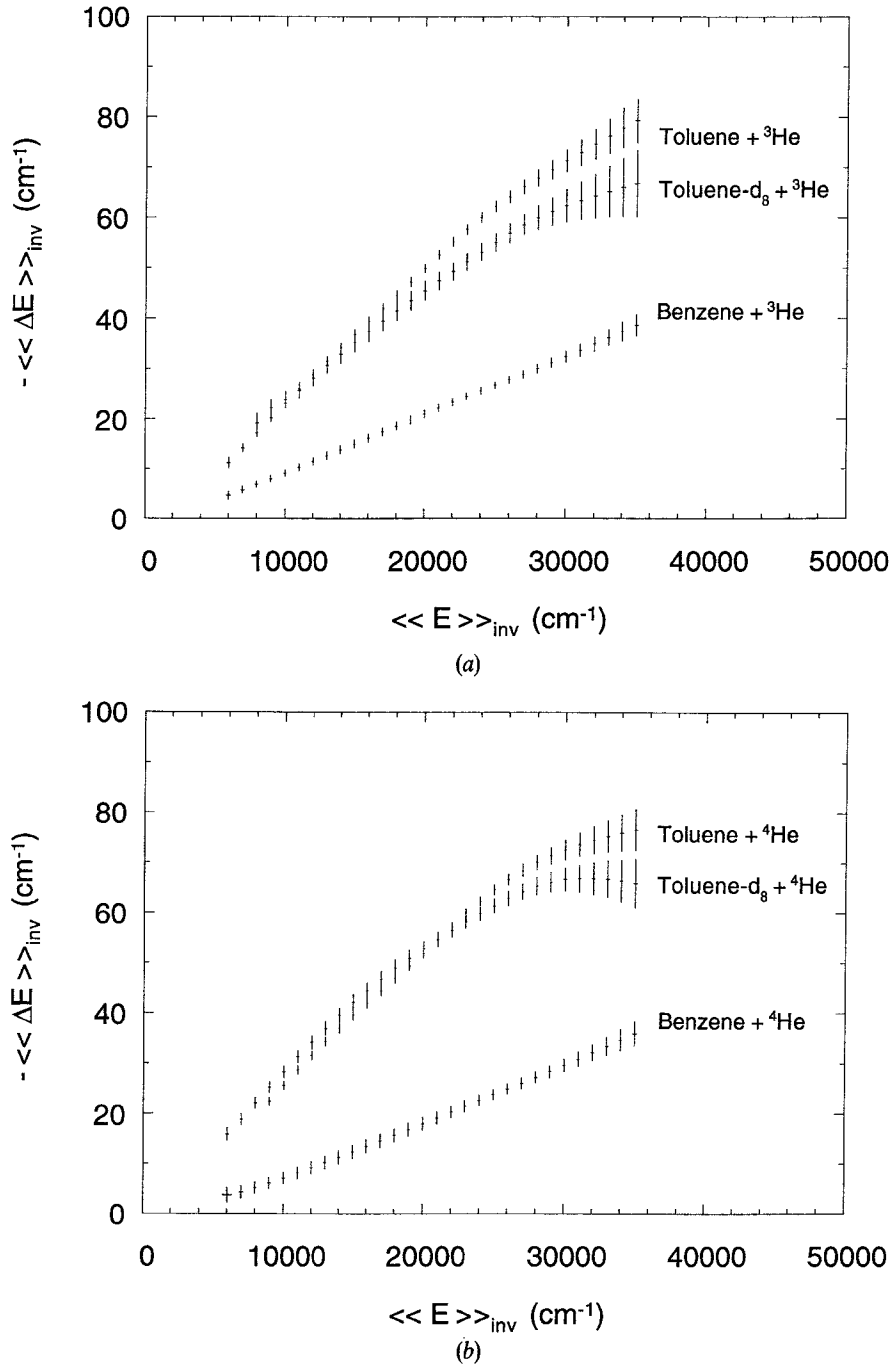

Figure 15. Average energy transferred per collision as a function of the average vibrational energy for isotopically substituted benzene derivatives deactivated in collisions with ^{3}He and ^{4}He (Toselli and Barker 1990, 1992).

energy in each vibration mode is equal: equipartition of energy. In a quantum system, however, this is not the case: the high frequency modes in a quantum system are 'energy poor', while the low frequency modes are 'energy-rich', as shown in figure 16. Classical equipartition of energy is not a good approximation, unless all of the modes contain a large amount of energy, relative to $h\nu_i$, or unless the vibrational frequencies are nearly degenerate. Furthermore, the zero-point energy is not constrained in classical systems, and when it is included along with the disposable vibrational energy in classical trajectory calculations, the high frequency modes contain far too much vibrational energy. These effects combine to introduce a fundamental bias in classical trajectory calculations involving large molecules which possess a typical range of vibrational frequencies.

For benzene-d_0 containing $\sim 10\,000\,cm^{-1}$ of vibrational energy in addition to the zero-point energy, the classically disposable average energy per mode is $\sim 1050\,cm^{-1}$, which can be compared with the $\sim 58\,cm^{-1}$ available in each C–H stretching mode in the corresponding quantum system. This effect is familiar from the Whitten–Rabinovitch expressions for quantum state sums and densities, where the zero-point energy appears explicitly and the parameter $a(E)$ depends on the distribution of vibrational mode fundamental frequencies. If these factors are neglected, the resulting classical expression provides a very poor approximation to the quantum sums and densities of states over reasonable ranges of energy (Robinson and Holbrook 1972, Forst 1973, Gilbert and Smith 1990).

It has been argued (Gilbert and Smith 1990, Gilbert 1991) that large molecules behave essentially classically, because of their high densities of states. In the limit of very high energies, this conclusion is correct, but most molecules studied at chemically accessible energies have not reached the high-energy classical limit. It is the inadequacy

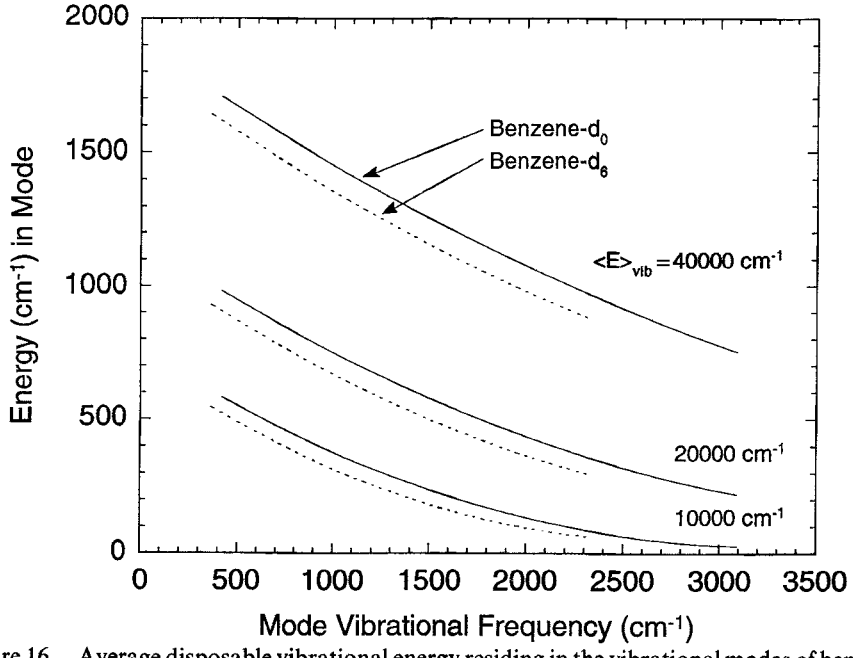

Figure 16. Average disposable vibrational energy residing in the vibrational modes of benzene-d_0 and benzene-d_6 according to quantum statistics (equation (6)), when the total disposable vibrational energy is 10 000, 20 000, and 40 000 cm^{-1} (Toselli and Barker 1992).

of the classical limit in describing quantum systems at chemical energies that leads to the bias discussed above. Note that the bias is less severe at high total energy and for smaller molecules (with a similar distribution of mode frequencies), but the bias is always present and may contribute to the successes and failures of classical trajectory simulations. Recent classical trajectory calculations on deuterated azulene (Clarke and Gilbert 1992) agree with experiments on deuterated benzene and toluene (Toselli and Barker 1992) in that there is little change in energy transfer due to the isotopic substitution. This result may indicate either that the classical statistical bias is not important, or that there are compensating errors; further research on this problem is needed.

7.2. V–T/R *and* V–V *energy transfer mechanisms*

Because the simple dipole–dipole model gives a good description of the experimental data involving CO_2, calculations were made to predict the amount of vibrational energy transferred to the bending mode of CO_2 (the symmetric stretch is symmetry-forbidden) from excited benzene. The dipole–dipole model predicts that much more energy will end up in the bending mode of CO_2 than in the asymmetric stretch. Specifically the population ratio $N^*_{\text{bending}}/N^*_{\text{asym}} \approx 100$ and V–V energy transfer to the bending mode contributes $\sim 10\%$ of the total $\langle\langle \Delta E \rangle\rangle$, when $E = 40\,000\,\text{cm}^{-1}$. The contributions of V–V energy transfer to the CO_2 bend and asymmetric stretch are shown in figure 17, along with the experimental measurements of $\langle\langle \Delta E \rangle\rangle_{\text{inv}}$. The calculated results are in reasonable agreement with other studies (Jalenak *et al.* 1988) and the model predicts that V–V energy transfer to the bending mode of CO_2 and V–T/R energy transfer are the two dominant mechanisms. The conclusion that V–T/R energy transfer is probably the most important mechanism for deactivating these highly vibrationally excited species is consistent with the conclusion reached by Lin and Rabinovitch (1970) more than 20 years ago.

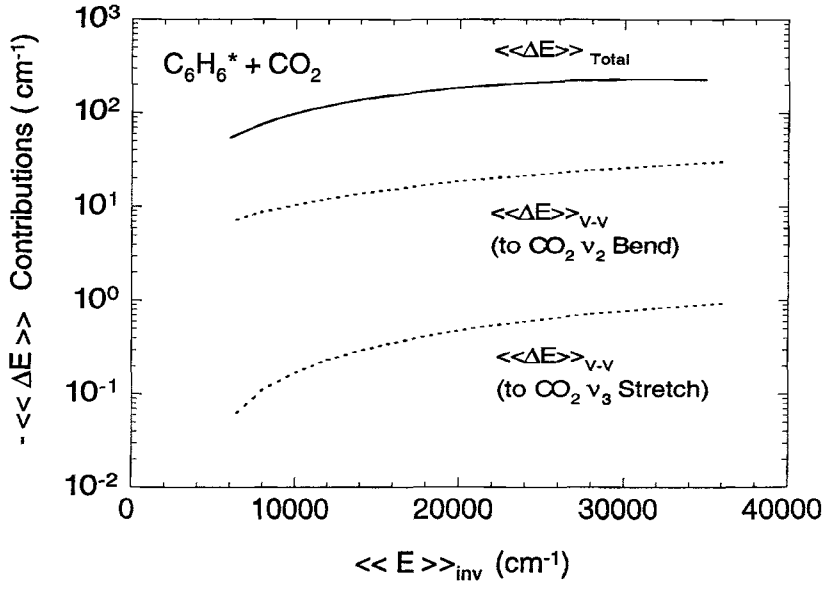

Figure 17. Estimated contributions of V–V energy transfer to $\langle\langle \Delta E \rangle\rangle_{\text{inv}}$ as a function of $\langle\langle E \rangle\rangle_{\text{inv}}$ for benzene-d_0 + CO_2 (Toselli and Barker 1991).

In the case of collisions with CO_2, V–T/R energy transfer is most likely dominant, but for other systems (parent–parent collisions, in particular) the relative importance of the V–V and V–T/R processes is not yet clear. The third component listed above is a logical extension of the simple theoretical model and it may explain why polar colliders produce larger $\langle\langle\Delta E\rangle\rangle$ values than non-polar species of comparable size. If this mechanism is indeed important, energy transfer involving polar collider gases is likely to produce highly excited rotational distributions in the collider gases, which may be observable using time-resolved spectroscopic techniques. Future work should address questions regarding the relative importance of V–V and $-T/R$ energy transfer, and the possible role of V–R energy transfer involving polar species.

Isotope effects can also be used to discern the likely roles of V–V and V–T/R energy transfer. The effects of deuteration (Toselli and Barker 1992) are presented in figure 16, which compares the average energy in each mode of benzene-d_0 and benzene-d_6, based on quantum statistics). Only the *higher* frequency modes are affected significantly by deuteration: the C–D stretch mode frequencies are about $2^{-1/2}$ times as large as those for the C–H stretches and the mode energy contents are increased slightly. The *lower* frequency modes are practically unaffected: their frequencies and their average energy contents are lowered only slightly by deuteration.

We conclude from figure 16 that if collisional energy transfer occurs mostly by V–T/R transfer from the lowest frequency modes, as expected from the Born approximation and Schwartz–Slawsky–Herzfeld theory (SSH) (Schwartz *et al.* 1952, Tanczos 1959, Yardley 1980), there will be little effect due to deuteration as long as intramolecular vibrational redistribution of energy is slow, relative to the duration of a collision. Most of the experimental data presented in figure 18 are consistent with this notion, as are recent classical trajectory calculations (Clarke and Gilbert 1992). The slight decrease in $\langle\langle\Delta E\rangle\rangle_{inv}$ for the deuterated isotopomers relative to the corresponding normal species for most colliders may be due in part to the slight lowering of

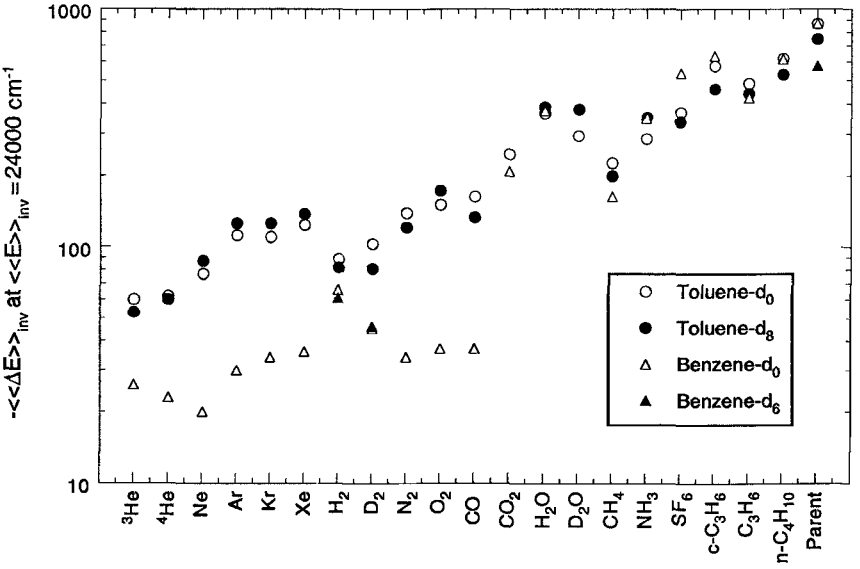

Figure 18. A comparison of the average energy transferred per collision (at $\langle E\rangle_{inv} = 24\,000\,cm^{-1}$) in deactivating benzene and toluene isotopomers (Toselli and Barker 1992).

average energy content in the low frequency modes in the deuterated molecules at the same total energy. This does not explain the larger effects seen for deactivation by the parent gases, however, where 'sticky collisions' and V–V energy transfer may be more important (figure 19).

In the isotopically substituted parent molecules, the dipole transition matrix elements are much weaker than in CO_2, and even though the vibrational frequencies of excited parent and collider match closely (but not exactly! see Brenner and Barker 1992a), the simple model indicates that V–V energy transfer is insignificant, if the IVR rates that fitted the CO_2 results are used. (The IVR rates are very uncertain, however.) This result provides indirect support for the conclusion that there is little contribution from V–V transfer, yet it does not help to explain the deuterium isotope effect observed for the parent gas colliders. Perhaps the durations of collisions involving large polyatomic colliders are significantly longer than the straight line trajectories assumed in the simple model.

The origin of the unusual $\langle\langle E\rangle\rangle_{inv}$ energy dependence observed for the deuterated species is not yet clear, but it could arise from resonance effects, if V–V energy transfer is more important than was concluded in the preceding paragraphs. If the vibrational transition energies in the highly excited species are anharmonically shifted, as has been observed for the benzene C–H stretching modes (Brenner and Barker 1992a), the excited species frequencies will shift further out of resonance with the unexcited species as the energy of the former is increased, possibly reducing the efficiency of energy transfer. This explanation is highly conjectural and requires that V–V energy transfer makes a significant contribution, contrary to the conclusions reached above. Until more definitive conclusions are reached about the mechanisms for energy transfer, this remains an open question.

Lendvay and Schatz (1992b) investigated the mechanisms of energy transfer with classical trajectory calculations concerning the deactivation of vibrationally excited

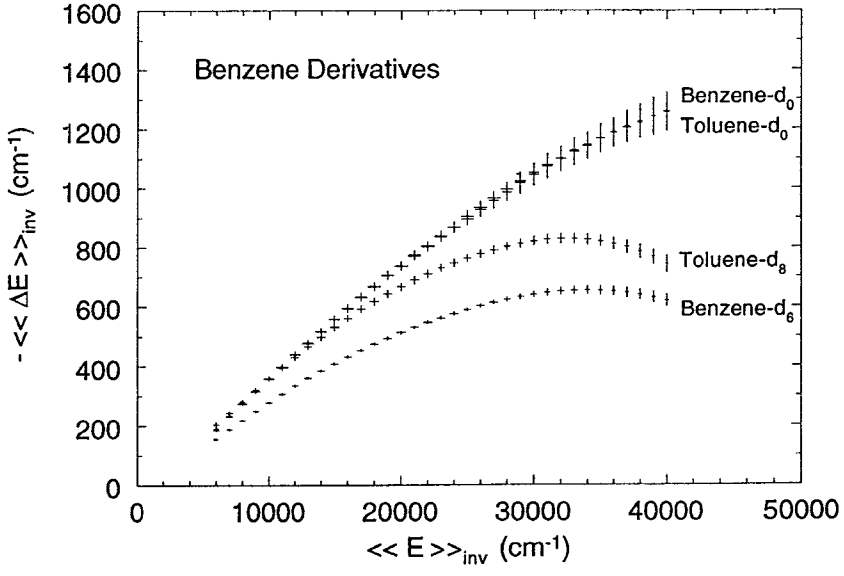

Figure 19. Average energy transferred per collision as a function of the average vibrational energy for isotopically substituted benzene derivatives deactivated in collisions with the unexcited species (Toselli and Barker 1992).

SF_6 in collisions with monatomic, diatomic, and polyatomic gases. They found relatively complex behaviour: *V–T* and *V–R* transfer dominates for small colliders, but *V–V* transfer dominates in $SF_6^* + SF_6$ collisions. Our conclusion that *V–T/R* transfer dominates in the experiments on benzene derivatives is based on results for small species and is extended to larger colliders. Our problems in explaining the 'roll-off' of $\langle\langle \Delta E \rangle\rangle$ at high energies are solved if the mechanism for energy transfer changes dramatically for larger colliders, as indicated by the calculations of Lendvay and Schatz (1992b). This is an important area for more research.

More experiments are needed to determine the importance of *V–V* energy transfer in collisions involving two polyatomics. It seems possible that the majority of energy transfer collisions involve *V–T/R* transfer of relatively small energies, but a small fraction of collisions transfer significantly larger amounts of energy by *V–V* transfer. If this conjecture is correct, *V–V* energy transfer may contribute to 'supercollisions', in which surprisingly large amounts of energy are transferred (Hassoon *et al.* 1988, Löhmannsröben and Luther 1988, Luther and Reihs 1988, Pashutzi and Oref 1988, Morgulis *et al.* 1989, Lendvay and Schatz 1990, 1992a).

Acknowledgments

For financial support, we thank the U.S. Department of Energy, Office of Basic Energy Research, and B.M.T. thanks CONICET for a Postdoctoral Fellowship for part of her stay at the University of Michigan. We also thank all of our co-authors on the original publications that are reviewed here: Diane Bernfeld, Jichun Shi, Murthy L. Yerram, Jerrell D. Brenner, William E. Chin, and Keith D. King.

References

ASTHOLZ, D. C., TROE, J., and WEITERS, W., 1979, *J. chem. Phys.*, **70,** 5107.

ATKINSON, R., and THRUSH, B. A., 1969, *Chem. Phys. Letters*, **3,** 684; 1970, *Proc. R. Soc.* A, **316,** 123, 131, 143.

BARKER, J. R., 1983, *Chem. Phys.*, **77,** 201; 1984, *J. phys. Chem.*, **88,** 11; 1992, *Ibid.*, **96,** 7361.

BARKER, J. R., and GOLDEN, R. E., 1984, *J. phys. Chem.*, **88,** 1012.

BARKER, J. R., ROSSI, M. J., and PLADZIEWICZ, J. R., 1982, *Chem. Phys. Lett.*, **90,** 99.

BEVILACQUA, T. J., ANDREWS, B. K., STOUT, J. E., and WEISMAN, R. B., 1990, *J. chem. Phys.*, **92,** 4627.

BEVINGTON, P. R., 1969, *Data Reduction and Error Analysis for the Physical Sciences* (New York: McGraw-Hill), p. 237.

BEYER, T., and SWINEHART, D. F., 1973, *Commun. Assoc. Comput. Mach.*, **16,** 379.

BRENNER, J. D., and BARKER, J. R., 1992a, *Astrophys. J. Lett.*, **388,** L39; 1992b, (manuscript in preparation).

BRUEHL, M., and SCHATZ, G. C., 1988a, *J. chem. Phys.*, **89,** 770; 1988b, *J. phys. Chem.*, **92,** 7223.

CAMY PEYRET, C., and FLAUD, J. M., 1985, *Molecular Spectroscopy: Modern Research*, Vol. III, edited by K. Nakahari Rao (New York: Academic Press).

CHERCHNEFF, I., and BARKER, J. R., 1989, *Astrophys. J. Lett.*, **341,** L21.

CHOU, J. Z., HEWITT, S. A., HERSHBERGER, J. F., and FLYNN, G. W., 1990, *J. chem. Phys.*, **93,** 8474.

CHOU, J. Z., HEWITT, S. A., HERSHBERGER, J. F., BRADY, B. B., SPECTOR, G. B., CHIA, L., and FLYNN, G. W., 1989, *J. chem. Phys.*, **91,** 5392.

CLARKE, D. L., and GILBERT, R. G., 1992, *J. phys. Chem.*, **96,** 8450.

COTTRELL, T. L., and MCCOUBREY, J. C., 1961, *Molecular Energy Transfer in Gases* (London: Butterworths).

DURANA, J. F., and MCDONALD, J. D., 1976, *J. chem. Phys.*, **64,** 2518.

FORST, W., 1973, *Theory of Unimolecular Reactions* (New York: Academic Press).

FORST, W., and BARKER, J. R., 1985, *J. chem. Phys.*, **83,** 124.

FÖRSTER, T., 1965, *Mod. quant. Chem.*, **3,** 93.

GILBERT, R. G., 1991, *Int. Rev. phys. Chem.*, **10,** 319.

GILBERT, R. G., and SMITH, S. C., 1990, *Theory of Unimolecular and Recombination Reactions* (Oxford: Blackwell Scientific), Chap. 5.

GILBERT, R. G., and ZARE, R. N., 1990, *Chem. Phys. Letters*, **174**, 304.
HALLER, I., and SRINAVASAN, R., 1965, *J. chem. Phys.*, **42**, 2977.
HASSOON, S., OREF, I., and STEEL, C., 1988, *J. chem. Phys.*, **89**, 1743.
HIPPLER, H., and TROE, J., 1989, *Bimolecular Collisions*, edited by J. E. Baggott and M. N. Ashfold (London: The Royal Society of Chemistry), p. 209.
HIPPLER, H., TROE, J., and WENDELKIN, H. J., 1981, *Chem. Phys. Letters*, **84**, 257; 1983, *J. chem. Phys.*, **78**, 6709, 6718.
HUDDLESTON, R. K., FUJIMOTO, G. T., and WEITZ, E., 1982, *J. chem. Phys.*, **76**, 3839.
JALENAK, W., WESTON, R. E. JR, SEARS, T. J., and FLYNN, G. W., 1988, *J. chem. Phys.*, **89**, 2015.
KOHLMAIER, G., and RABINOVITCH, B. S., 1963, *J. chem. Phys.*, **38**, 1692, 1709.
KRAJNOVICH, D. J., PARMENTER, C., and CATLETT, D. L. JR, 1987, *Chem. Rev.*, **87**, 237.
LAMBERT, J. D., 1977, *Vibrational and Rotational Relaxation in Gases* (Oxford: Clarendon Press).
LENDVAY, G., and SCHATZ, G. C., 1990, *J. phys. Chem.*, **94**, 8864; 1992a, *Ibid.*, **96**, 4356; 1992b, *J. chem. Phys.* (to be published).
LIM, K. F., and GILBERT, R. G., 1990, *J. phys. Chem.*, **94**, 72, 77.
LIN, Y. N., and RABINOVITCH, B. S., 1970, *J. phys. Chem.*, **74**, 3151.
LINDEMANN, F. A., 1922, *Trans. Faraday Soc.*, **17**, 598.
LÖHMANNSRÖBEN, H. G., and LUTHER, K., 1988, *Chem. Phys. Lett.*, **144**, 473.
LUTHER, K., 1992, private communication.
LUTHER, K., and REIHS, K., 1988, *Ber. Bunsenges. phys. Chem.*, **92**, 442.
LUU, S. H., and TROE, J., 1974, *Ber. Bunsenges. phys. Chem.*, **78**, 766.
MAHAN, B. H., 1967, *J. chem. Phys.*, **46**, 98.
MOORE, C. B., 1973, *Adv. chem. Phys.*, **23**, 41.
MORGULIS, I. M., SAPERS, S. S., STEEL, C., and OREF, I., 1989, *J. chem. Phys.*, **90**, 923.
NAKASHIMA, N., and YOSHIHARA, K., 1982, *J. chem. Phys.*, **77**, 6040; 1983, *Ibid.*, **79**, 2727.
NEPORENT, B. S., 1950, *Zh. Fiz. Khim.*, **24**, 1219.
NEPORENT, B. S., and MIRUMYANTS, S. O., 1960, *Opt. Spectrosc. USSR*, **8**, 336.
OREF, I., and TARDY, D. C., 1990, *Chem. Rev.*, **90**, 1407.
ORR, B. J., and SMITH, I. W. M., 1987, *J. phys. Chem.*, **91**, 6106.
PASHUTZKI, A., and OREF, I., 1988, *J. phys. Chem.*, **92**, 178.
PENNER, A. P., and FORST, W., 1977, *J. chem. Phys.*, **67**, 5296.
QUACK, M., and TROE, J., 1977, *Gas Kinetics and Energy Transfer* (London: Chem. Soc.), Vol. 2.
RABINOVITCH, B. S., CARROLL, H. F., RYNBRANDT, J. D., GEORGAKAKOS, J. H., THRUSH, B. A., and ATKINSON, R., 1971, *J. phys. Chem.*, **75**, 3376.
RAWLINS, W. T., CALEDONIA, G. E., GIBSON, J. J., and STAIR, A. T. JR, 1985, *Geophys. Res. Lett.*, **90**, 2896.
ROBINSON, P. J., and HOLBROOK, K. A., 1972, *Unimolecular Reactions* (London: Wiley).
ROSSI, M. J., and BARKER, J. R., 1982, *Chem. Phys. Lett.*, **85**, 21.
ROSSI, M. J., PLADZIEWICZ, J. R., and BARKER, J. R., 1983, *J. chem. Phys.*, **78**, 6695.
SCHWARTZ, R. N., SLAWSKY, Z. I., and HERZFELD, K. F., 1952, *J. chem. Phys.*, **20**, 1591.
SEDLACEK, A. J., WESTON, R. E., and FLYNN, G. W., 1991, *J. chem. Phys.* **94**, 6483.
SHI, J., and BARKER, J. R., 1988, *J. chem. Phys.*, **88**, 6219; 1990, *Int. J. chem. Kinetics*, **22**, 187.
SHI, J., BERNFELD, D., and BARKER, J. R., 1988, *J. chem. Phys.*, **88**, 6211.
SMALLEY, R. E., 1983, *Ann. Rev. phys. Chem.*, **34**, 129.
SMITH, G. P., and BARKER, J. R., 1981, *Chem. Phys. Lett.*, **78**, 253.
STEIN, S. E., and RABINOVITCH, B. S., 1973, *J. chem. Phys.*, **58**, 2438.
TANCZOS, F. I., 1959, *J. chem. Phys.*, **30**, 1119.
TARDY, D. C., and RABINOVITCH, B. S., 1977, *Chem. Rev.*, **77**, 369.
TOSELLI, B. M., and BARKER, J. R., 1990, *Chem. Phys. Lett.* **174**, 304; 1991, *J. chem. Phys.*, **95**, 8108; 1992, *Ibid.*, **97**, 1809.
TOSELLI, B. M., WALUNAS, T. L., and BARKER, J. R., 1990, *Chem. Phys. Lett.* **92**, 4793.
TOSELLI, B. M., BRENNER, J. D., YERRAM, M. L., CHIN, W. E., KING, K. D., and BARKER, J. R., 1991, *J. chem. Phys.*, **95**, 176.
WEITZ, E., and FLYNN, G. W., 1974, *Ann. Rev. phys. Chem.*, **25**, 275.
WHITTEN, G. Z., and RABINOVITCH, B. S., 1964, *J. chem. Phys.*, **41**, 1883.
YARDLEY, J. T., 1980, *Introduction to Molecular Energy Transfer* (New York: Academic Press).
YERRAM, M. L., BRENNER, J. D., KING, K. D., and BARKER, J. R., 1990, *J. phys. Chem.*, **94**, 6341.
ZELLWEGER, J. M., BROWN, T. C., and BARKER, J. R., 1985a, *J. chem. Phys.*, **83**, 6251; 1985b, *Ibid.*, **83**, 6261; 1986, *J. phys. Chem.*, **90**, 461.